Ref. Ares(2025)6601671 - 14/08/2025

MINAGRIS

Deliverable 5.2

Report of modelling transport of MNP in soil

Document Control Information

Settings	Value
Deliverable Title	Report of modelling transport of MNP in soil
Work Package Title	WP5: Assessment of the impact of MNP and combined effects with other stressors on soil physical and chemical properties and crop productivity

Deliverable number	5.2
Description	Report
Lead Beneficiary	University of Bern (UBERN)
Lead Authors	Abdallah Alaoui
Contributors	Rozita Soltani Tehrani, Adrian Grunder, Sinh Ly
Submitted by	Esperanza Huerta Lwanga
Doc. Version (Revision number)	2
Sensitivity (Security):	Public after 6 months embargo
Date:	14/08/2025

Document Approver(s) and Reviewer(s):

NOTE: All Approvers are required. Records of each approver must be maintained. All Reviewers in the list are considered required unless explicitly listed as Optional.

Name	Role	Action	Date
Esperanza Huerta Lwanga	Co-coordinator	Reviewer	29-07-2025

Document history:

The Document Author is authorized to make the following types of changes to the document without requiring that the document be re-approved:

- Editorial, formatting, and spelling
- Clarification

Configuration Management: Document Location

The authors expressed the need to keep this document confidential until their scientific paper is published. They ask for a period of 6 months embargo. Therefore, the location of this document is not yet public.

Nature of the deliverable		
R	Report	X
DEC	Websites, patents, filing, etc.	
DEM	Demonstrator	
O	Other	

Dissemination level		
PU	Public after 6 months embargo	
CO	Confidential, only for members of the consortium (including the Commission Services)	**X**

ACKNOWLEDGEMENT

This report forms part of the deliverables from the MINAGRIS project which has received funding from the European Union's Horizon 2020 research and innovation programme under Grant Agreement No. 101000407. The Community is not responsible for any use that might be made of the content of this publication.

MINAGRIS - MIcro- and NAno-Plastics in AGRIcultural Soils: sources, environmental fate and impacts on ecosystem services and overall sustainability– is an H2020 project funded under the H2020 Programme, coordinated by WAGENINGEN UNIVERSITY (WU).

The MINAGRIS project, launched on September 1st, 2021, aims to contribute to healthy soils in Europe by providing a deeper understanding and tools to assess the impact of MP and NP in agricultural soil health. To create an overview on the actual situation across Europe, MINAGRIS will assess the use of different plastic polymers in agricultural systems in 11 case study across Europe and identify the resulting types and concentrations of MPs and NPs. Concentrations of other stressors in soils such as pesticides and veterinary drugs will be additionally assessed. MINAGRIS will provide validated analytical tools that allow the quantification and identification of MPs and NPs in European agricultural soils.

The project, funded by the EU Research and Innovation Programme Horizon 2020 under Grant Agreement n. 101000407 gathers 20 partnering organisations from 12 EU Member States with various biogeographical regions, and they are representative of different farming systems and soils across Europe. It has an overall budget of approximately €7 million and will run for 5 years, between September 2021 and September 2026.

More information on the project can be found at: https://www.minagris.eu

TABLE OF CONTENTS

ACKNOWLEDGEMENT **3**
TABLE OF CONTENTS **4**
LIST OF ABBREVIATIONS **5**
LIST OF FIGURES **6**
LIST OF TABLES **6**
EXECUTIVE SUMMARY **7**
1. INTRODUCTION **9**
2. MATERIAL AND METHODS **10**
2.1. Experimental and modelling of MPs in reconstructed soil columns 10
2.1.1. Construction of soil columns 10
2.1.2. Experiments 10
2.1.3. Soil hydraulic matrix parameters 11
2.1.4. Modelling 11
2.2. Modelling MP transport in reconstructed soil under natural conditions 11
2.2.1. Experiment I. Wageningen University. 11
2.2.3. Particle counting 12
2.2.3. Treatments and soil collection 13
2.3. Transport of MP in undisturbed soil under natural conditions (Experiment II.Tillage impact interaction, Switzerland) 14
2.3.1. Treatments 14
2.3.2. Installation of lysimeters 14
2.3.3. Description of the MP infiltration 15
2.3.4. Dye tracer experiments 16
2.3.5. Sampling design 16
3. RESULTS **18**
3.1. Experimental and modelling of MP in reconstructed soil columns 18
3.2. Modelling MP transport in reconstructed soil under natural conditions (Experiment I, Wageningen University). 26
3.3. Experimental and modelling MP in undisturbed soil under natural conditions (Experiment II. Switzerland). 29
3.3.1. Laboratory results 29
3.3.2. Meteorological data 30
3.3.3. Microplastic analysis 31
3.3.4. Dye tracer analysis 37
3.3.5. Earthworm activity 37
4. SUMMARY AND CONCLUSIONS **40**
5. LIST OF REFERENCES **42**
6. ANNEXE 1 ..... **44**

LIST OF ABBREVIATIONS

CEC	Cation exchange capacity
CL	Clay-loam soil type
CNS	Carbon, Nitrogen, Sulphur
HDPE	High-Density Polyethylene
GWC	Gravimetric Water Content
ISO	International Organization for Standardization.
Ksat	Saturated Hydraulic Conductivity
LDPE	Low density polyethylene;
LOI	Loss On Ignition
MINAGRIS	MINAGRIS Micro- and Nano-Plastics in Agricultural Soils (Project)
MNP	Micro- nano plastic
MP	Microplastic
OM	Organic Matter
PBAT	Polybutylene adipate terephthalate
PE	Polyethylene
PET	Polyethylene Terephthalate
pF	Potential force, describes the effort it takes the plants' roots to extract water from the soil
PP	Polypropylene
PS	Polystyrene
PU	Polyurethane
PVC	Polyvinyl Chloride
SOP	SOP Standard Operation Procedure
TDR	Time Domain Reflectometry
TOC	Total Organic Carbon
TWP	Tire Wear Particles
VWC	Volumetric Water Content
WRC	Water Retention Curve

List of Figures

Figure 1. Experimental setup. 13
Figure 2. Study field in Unterzollikofen (BE) Switzerland (Lat.: 46.989, Lon.: 7.462, 560 m a.s.l.), separated in two subfields with different management practices (till and no-till). The red dot in the aerial image indicates the exact location of the datalogger. 14
Figure 3. Overview of the experimental set up in Unterzollikofen (BE) (own work, 2024). 16
Figure 4. Sketch of the dye tracer location on the study field. L1 refers to lysimeter in field 1. L2 refers to lysimeter in field 2, respectively, A and B refer to control and spiked lysimeters, respectively 16
Figure 5. Aerial view of the lysimeter, showing 4 sampling bore holes, drilled with a sampling auger (taken on 13.12.2024). 17
Figure 6. Observed and simulated breakthrough curves for different treatments. LS = loamy sand, SL = sandy loam, H = high rainfall intensity (35 mm/h), and L = low rainfall intensity (22 mm/h). 20
Figure 7. Observed and simulated retention profile for all treatments. LS = loamy sand, SL = sandy loam, H = high rainfall intensity (35 mm/h), and L = low rainfall intensity (22 mm/h) 24
Figure 8. Observed and simulated retention profile for all treatments, averaged across replicates 26
Figure 9. Observed and simulated retention profile for all treatments, averaged across replicates 30
Figure 10. Rain and calibrated soil moisture data in field 2 (no-till) 31
Figure 11. Graph showing the difference between the result for the uncorrected microplastic concentration values and the corrected values 32
Figure 12. Results for microplastic concentration per depth in lysimeter A and B of field 1 (till) in particle/g 33
Figure 13. Results for microplastic concentration per depth in lysimeter A and B of field 2 (no-till) in particle/g 34
Figure 14. Calculated average concentration values per depth from lysimeters A and B of the respective fields 35
Figure 15. Average MP size distribution of lysimeters A and B of field 1 (till) 36
Figure 16. Average MP size distribution of lysimeter A and B of field 2 (no-till) 36
Figure 17. Processed images of soil profiles retrieved from the dye tracer experiment. The water colors are highlighted to accommodate visual interpretation 37
Figure 18. Illustration of earthworm burrows in Field 2, depth 0-20 cm 39

List of Tables

Table 1. Initial particle size distribution of microplastics (%) 12
Table 2. Microplastic input concentrations for field 1 and field 2. 15
Table 3. Optimization of VGM parameters for each soil type using the evaporation method, and dispersivity values using tracer experiments. 18
Table 4. Fitted model parameters. 25
Table 5. Fitted model parameters after field experiment I. 27
Table 6. Overview of the soil properties in field 1 (till) and 2 (no-till). 29
Table 7. Detailed overview of Ksat results, showing number of samples and standard deviation for field 1 (till) and field 2 (no-till). 29
Table 8. Overview of the retrieved Van Genuchten parameters for field 1 (till) and field 2 (no till). 29
Table 9. Ksat values affected by earthworm burrow (red), unaffected (green) and low impacted (orange). 38
Table 10. Bulk density values for soil texture classes. 44

EXECUTIVE SUMMARY

Microplastics exist both as primary and secondary contaminants. Primary microplastics are manufactured to be smaller than 5 mm (mostly industrial abrasives and care products) and directly enter the environment. In contrast, secondary microplastics are the product of environmental degradation of large-sized plastic pieces. Secondary microplastic particles are not produced intentionally but are the result of the breakdown and fragmentation of plastic particles via biological, physical, and chemical processes. The widespread contamination in the environment is due to the increasing use of plastic materials in agriculture—especially plastic mulch films and compost—which has led to growing concerns about the accumulation of microplastics (MP) and nanoplastics (NP) in agricultural soils. When microplastics are released into the terrestrial environment, they can be aged by thermally initiated oxidative degradation, hetero aggregation, as well as bioturbation. Ageing affects the physicochemical properties, including the increase of surface roughness and oxygen-containing groups. This can further enhance the sorption capability, thus increasing microplastic mobility in the soil.

This deliverable aims to measure and model advanced physical properties (e.g. soil water dynamics), their effects on MP transport in combination with soil biota reaction and activity on representative soil types from selected fields.

More specifically, D5.2 will investigate the degree of preferential flow qualitatively (e.g., using dye tracer experiments) and quantitatively by analyzing the amount of MP in the soil and modelling under laboratory and field conditions.

We aimed at improving the understanding of NP transport in soils and to gain insights into the principal physicochemical mechanisms, as well as the experimental conditions (e.g. degree of saturation, flow rate, particle concentration, and size) governing their mobility and retention.

Deliverable 5.2 evaluates how MPs—including conventional plastics (LDPE), biodegradable types (PBAT), and biobased alternatives (starch-based MP)— are transported downward in the soil profile and what factors are governing their movement.

The results of the laboratory soil columns showed that parameter variations from inverse modelling illustrated differences in microplastic attachment rates and dispersivity across treatments, with high retention in the fine texture. Under natural conditions, LDPE exhibited high stability, with minimal changes in retention profiles and particle size distributions over time, reflecting its resistance to biodegradation and fragmentation. In contrast, PBAT and starch-based microplastics demonstrated more dynamic behaviour. Land use also impacts the MP (LDPE) transport in soil.

At field conditions, tillage had a significant impact on soil structure and water flow, illustrated by the increasing microplastic penetration depth with the abundance of macropores, highlighting the importance

of preferential flow paths for microplastic mobility. The highest mobility of plastic particles was detected at a depth of 0-15 cm, while a large percentage of microplastics fail to penetrate the tilled soil after 5.5 months due to the high retention of top-10 cm compacted soil.

This deliverable is structured as follows:

1. Experimental and modelling of MPs in reconstructed soil columns
2. Modelling MP transport in reconstructed soil under natural conditions
3. Experimental and modelling MP in undisturbed soil under natural conditions

1. INTRODUCTION

Microplastics can move in different ways when entering the soil. The horizontal movement of microplastics can be influenced by soil biota activity as well as soil properties. Further, ploughing, harvesting, and bioturbation are causes of microplastic transport in the subsurface of the soil. Factors influencing the mobility of microplastic in the soil are the properties of microplastic, such as type, particle size, shape, density, and surface chemistry. Environmental factors include soil pH, ionic strength, cation type, mineral contents, organic matter, wet-dry cycle, freeze-thaw cycle, flow rate, co-existing engineered nanoparticles, surfactants, and bacterial effects (Ren et al., 2021). The mobility of microplastic is dependent on its surface characteristics, especially hydrophobicity and functional groups (Ren et al., 2021 and Dong et al., 2019).

Contaminants can enter the soil through various pollution pathways and their transport is governed by various mechanisms depending on soil textural and structural porosity (Alaoui et al., 2011). Colloids are nanometer- or micrometer-sized particles [traditionally defined as between 1 nm and 10 µm (Rhodes, 2008). The transport of colloids through porous media is relevant to a wide range of fields such as medical sciences, industrial manufacturing, geosciences and environmental engineering. The transport of colloidal particles (particles with a size between 0.001 and 1 µm) in porous media is governed by complex mechanisms that influence their movement, retention, and remobilization. These mechanisms are essential for understanding the fate of pollutants in natural environments and designing effective remediation strategies. The key processes controlling colloid transport include attachment and detachment, straining, interception, sedimentation, and the influence of air-water and water-solid interfaces, particularly under transient flow conditions (Fig. 1.1). Colloidal particles can adhere to solid surfaces within porous media through physicochemical interactions, a process referred to as attachment (Tufenkji and Elimelech, 2004). Detachment, on the other hand, involves the release of these particles back into the aqueous phase. The balance between attachment and detachment significantly influences particle mobility and is governed by surface charge, hydrodynamic forces, and chemical conditions. The Derjaguin–Landau–Verwey–Overbeek (DLVO) theory provides a widely used framework for understanding these interactions, considering the balance between attractive van der Waals forces and repulsive electrostatic forces (Hahn et al., 2004; Tufenkji and Elimelech, 2005). However, deviations from the classical DLVO theory often occur due to surface heterogeneities, nanoscale roughness, and non-DLVO forces such as hydrophobic interactions (Bradford et al., 2007).

While several studies have investigated microplastic transport in the soil through both experimental and modelling approaches, most of them have focused on the behavior of pristine, spherical polystyrene particles with varying sizes and surface properties, typically in controlled porous media such as sand or glass beads (Mitzel et al., 2016; Tiraferri et al., 2011). Additionally, some research has explored non-spherical plastic particles within soil columns (Pradel et al., 2020; Xu et al., 2008; Yan et al., 2020), and only few field studies have examined microplastic transport under natural conditions. This study is aimed to advance predictive capabilities for microplastic release in unsaturated soil with transient water content. Specifically, we examined the influence of soil texture (sandy loam and loamy sand), microplastic type (LDPE, PBAT, and starch-based), and rainfall intensity on microplastic transport and retention, following the methodology of Tehrani et al. (2025). The findings offer valuable insights into how soil texture, rainfall

intensity, and microplastic characteristics interact and influence microplastic mobility, providing a more comprehensive understanding of microplastic behaviour in realistic environmental conditions.

2. MATERIAL AND METHODS

This deliverable investigates the transport of MPs in soil using laboratory and field experiments, and modelling using the dual-permeability model HYDRUS (Šimůnek et al., 2018). The experiments and modelling consist of 3 parts: **i)** experimental and modelling of MPs in reconstructed soil columns, **ii)** modelling MP transport in reconstructed soil under natural conditions, and **iii)** experimental and modelling MPs in undisturbed soil under natural conditions.

2.1. Experimental and modelling of MPs in reconstructed soil columns

2.1.1. Construction of soil columns

To investigate the transport of microplastics in soil, soil columns were constructed using polyvinyl chloride (PVC) tubes with an inner diameter of 11.5 cm. A metal mesh filter with a 1 mm pore size was positioned at the base of each column to prevent soil movement while allowing water and microplastic particles to pass through. Each column was filled to a height of 32 cm and uniformly packed with moist soil to achieve a bulk density of 1.5 g/cm^3. Tensiometers were installed at depths of 2 cm and 22 cm, while a water content probe was placed at 12 cm depth to monitor soil moisture dynamics. Two distinct soil types were used in the columns: sandy loam, composed of 4.6 % clay, 42.7 % silt, 52.7 % sand, and 4 % organic matter, and loamy sand, composed of 2 % clay, 20 % silt, 74 % sand, and 3.8 % organic matter. The top 10 cm of each column was blended with 0.15 % (w/w) of one type of microplastic either low-density polyethylene (LDPE), polybutylene adipate terephthalate (PBAT), or starch-based polymers, reflecting realistic environmental scenarios where microplastics predominantly accumulate in the upper soil layer.

2.1.2. Experiments

At laboratory conditions, two rainfall intensities (22 mm/h and 35 mm/h) were applied over two distinct events, corresponding to 2.5 pore volumes of the columns, with a 24-hour gap between the two rainfall episodes (at ambient temperature and field capacity). Effluent samples were collected to assess the temporal release of microplastics during and after the rainfall events. Following the rainfall events, the soil columns were dismantled, and soil samples were collected at varying depths to quantify the distribution of microplastics. Each treatment was replicated three times, and control columns without microplastics were also prepared for each soil type, resulting in a total of 42 soil columns. The microplastic particles were extracted from samples using density separation method according to MINAGRIS protocol and were identified using microscopy and Fourier-transform infrared spectroscopy (μ-FTIR). This comprehensive experimental setup, which included control columns and multiple replications for each soil type and microplastic type, provides robust data on the transport dynamics of different microplastics in two soil textures.

2.1.3. Soil hydraulic matrix parameters

Soil hydraulic matrix parameters for sandy loam and loamy sand soils were determined using the evaporation method (Romano and Santini, 1999). Soil samples were packed into cores with an 8 cm height and a 10.1 cm diameter. Four mini-tensiometers were installed at 2 cm intervals, positioned 1 cm from the top and bottom boundaries. Measured soil water pressure heads and evaporation rates were analyzed through calibration using HYDRUS-1D (Šimůnek et al., 1998), with the residual water content set to 0.02. The calibration involved optimizing the Van Genuchten Mualem (VGM) parameters based on the measured tensiometer data. Initial parameter values were derived with pedotransfer functions using the soil texture. The resulting VGM parameters were then used in subsequent experiments to represent the soil hydraulic function of the soil matrix per soil type. For more details are given in Tehrani et al. (2025).

2.1.4. Modelling

The HYDRUS-1D inverse solver was used to calibrate the microplastic transport parameters β and K_att using the observed breakthrough curves and retention profiles. To evaluate the goodness of model fit, the coefficient of determination R2 was checked. Under unsaturated flow conditions, both the water-solid interface and the air-water interface may function as adsorption sites for microplastic particles. Since we did not measure these interfaces separately, we modelled the combined effect of both as a single adsorption site. Additionally, depth-dependent deposition was enabled to account for immobile water zones, acknowledging that a fraction of the water in the soil column contributes minimally to particle transport. This approach reflects the natural heterogeneity of soil pore spaces where particles may temporarily be retained. By optimizing the β parameter we achieved a better fit with the measured retention data, accurately representing the observed particle distribution in the soil, especially in the top 10 cm.

In our modelling approach, some parameters were assigned fixed values based on preliminary optimization results. For example, Smax was set to 0.765, and Kdet to 1.55 × 10-5. These parameters showed minimal sensitivity during preliminary optimization, remaining effectively constant and unchanged throughout the process. Fixing these parameters allowed us to reduce model complexity and focus on optimizing the more sensitive parameters while maintaining a physically realistic representation of microplastic transport.

2.2. Modelling MP transport in reconstructed soil under natural conditions

2.2.1. Experiment I. Wageningen University.

To investigate microplastic transport in soil, we constructed soil columns using polyvinyl chloride (PVC) tubes with an inner diameter of 11.5 cm. A nonwoven geotextile cloth with a pore size of 0.12 mm and water permeability of 110 L m^{-2} s^{-1}, comparable to gravel, was placed at the bottom of each column to prevent earthworm intrusion and eliminate bioturbation during the experiment. The cloth did impose negligible hydraulic resistance. The columns were installed in the field at Unifarm, Wageningen University (51°59'22.4"N, 5°39'43.7"E), after creating holes with the same diameter as the PVC tubes (Fig. 5.1). Each

column was filled to a height of 32 cm with loamy sand soil (2% clay, 20% silt, 74% sand) containing 3.8% organic matter. The soil was uniformly packed to a bulk density of 1.5 g/cm³. The bottom 22 cm was packed with moist soil, while the top 10 cm was mixed with 0.15% (w/w) of one type of microplastic: low-density polyethylene (LDPE), polybutylene adipate terephthalate (PBAT), or starch-based polymer. For the control treatment, the same procedure was applied, without adding microplastic to the soil.

2.2.3. Particle counting

The particle counts per gram of polymer (mean ± SD, n = 20), quantified using a microscopic method as detailed in section 2.1.2, were as follows: LDPE (31,602 ± 60 particles/g, CV = 0.19%), PBAT (29,447 ± 70 particles/g, CV = 0.24%), and starch-based (13,552 ± 50 particles/g, CV = 0.37%). The size distribution of the microplastics added to the soil was measured and is presented in **Table 1**.

Table 1. Initial particle size distribution of microplastics (%)

Size range (µm)	PE (%)	PBAT (%)	Starch-based (%)
10-50	28.4	34.4	21.6
50-100	28.4	41.2	34.2
100-150	14.8	18.3	26.1
150-200	9.9	3.3	7.7
200-250	6.2	2.1	5.9
>250	12.3	0.7	4.5

Figure 1. Experimental setup.

2.2.3. Treatments and soil collection

Each treatment included six replicates. To study the effect of time on the degradation and transport of microplastics, three replicates were harvested 6 months after column installation, while the remaining three were harvested after 12 months. Meteorological data were collected from the Veenkampen weather station, 6.6 km from the study site near Wageningen University, Wageningen, the Netherlands. Groundwater levels were recorded using a pressure sensor (HYDROS 21, METER Group; resolution: 1 mm) installed in the field between the soil columns. Immediately after extraction from the ground, soil columns were removed entirely and mostly intact from the PVC tubes and laid gently upon a clean platform. Then, soil samples were collected at 5 cm intervals within the top 10 cm depth, corresponding to the microplastic source zone. Below this depth, the sampling interval was reduced to 2.5 cm.

Microplastic extraction and measurement after field experimentation

Following MINAGRIS protocol for quality control, after each set of 20 samples, two spiked samples were included containing the same type of microplastic used in the treatments, where the soil was mixed with a known quantity of microplastics. These spiked samples were processed using the same extraction method as the soil column samples, and the extracted microplastics were identified using a microscope. Blank samples were also included in the assessment. The recovery rates of the spiked samples ranged from 81% to 95% for LDPE, 74% to 88% for PBAT, and 73% to 82% for starch-based microplastics.

2.3. Transport of MPs in undisturbed soil under natural conditions (Experiment II. Tillage impact interaction, Switzerland)

The aim of this study is to gain a deeper understanding of the fate and behavior of microplastics in soils, focusing on their transport, accumulation, and potential interactions with soil structure and processes. By investigating key factors such as preferential flow, soil texture, soil properties, and macropore dynamics,

this research seeks to clarify the mechanisms driving microplastic movement within the soil profile under natural conditions.

2.3.1. Treatments

The study site is located on the Oberacker in Unterzollikofen (BE) in Switzerland. The location has an average yearly temperature of 9.3° C and an average yearly precipitation of 1109 mm. The study field is situated within a farming system characterized by a crop rotation strategy. Since 1993 no irrigation system was used on the field (Chervet et al., 2016). The fertilization regime involves the application of a mineral fertilizer at a rate of 750 kg per hectare. The crops included in the crop rotation systems are wheat, sugar beet, barley and field beans. During the entire investigation period of this study, the field was used for green manure.

The tillage was conventionally used on the **northern part** of the field to a depth of 25 cm until the year 2002. From 2003 an on-land plough was used, and from 2006 the tillage depth was reduced to 15 cm. On the **southern** part a direct seeding method is used. This separation of the field in two subfields started in 1994 as a long-term observation area (Chervet et al., 2016). Therefore, the study field can be separated into two subfields: field 1 with till, and field 2 has no till (**Figure 2**).

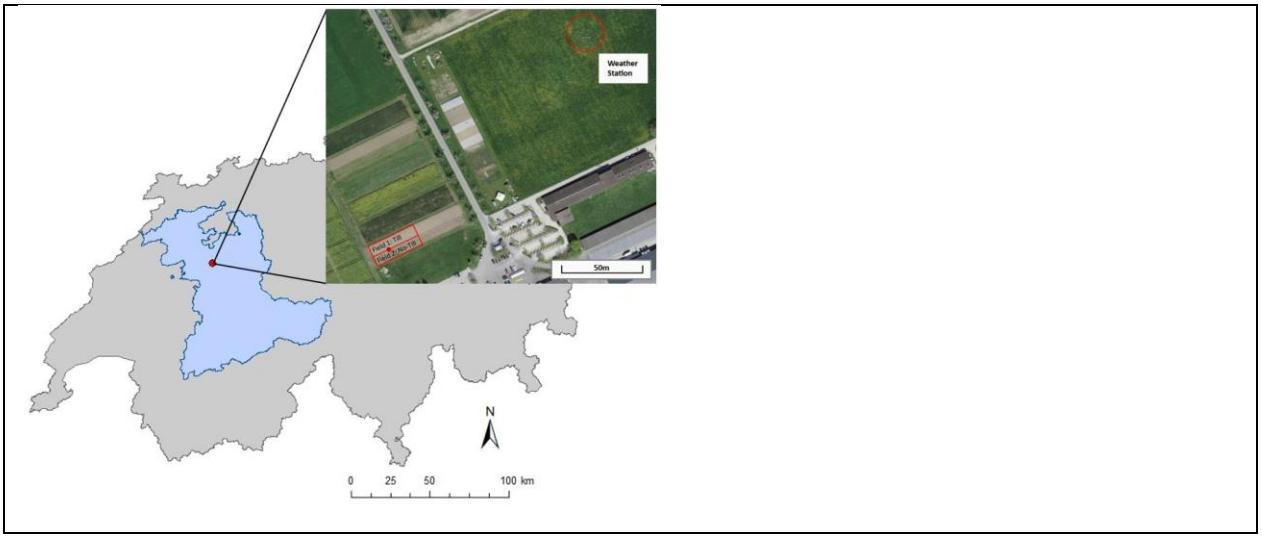

Figure 2. Study field in Unterzollikofen (BE) Switzerland (Lat.: 46.989, Lon.: 7.462, 560 m a.s.l.), separated in two subfields with different management practices (till and no-till). The red dot in the aerial image indicates the exact location of the datalogger.

2.3.2. Installation of lysimeters

Two lysimeters were installed in each field, with a distance of approximately 1.5 m between each other. Since only one lysimeter in each field is equipped with a moisture sensor, the small distance between the vessels ensures that soil moisture data can be used for the other non-equipped lysimeter as well, since the environmental conditions should be the same. The two fields have similar soil properties as the soil used in the soil column experiments from the University of Wageningen, conducted by Rozita Soltani, to allow further data comparison and validation. The lysimeter vessels used in this study are long cylinders with a diameter of 23 cm and a height of 35 cm. The inner diameter, excluding the 0.85 cm thick lysimeter walls,

is therefore 21.3 cm. This yields a volume of 11758.8 cm^3. ECH2O EC-5 soil moisture sensors are used to determine the soil water content. Lysimeter installation was completed on August 21, 2023. On the same day, exactly 1.03 g of low-density polyethylene < 250 µm was mixed with Milli-Q water and leaves from the field to avoid dispersal by wind and spiked on all four lysimeter soil surfaces. This concentration of LDPE was the same as the one used for the laboratory soil columns (**section 2.1**). Care was taken to distribute the LDPE plastic evenly on the entire surface area of the vessel. Upscaled to the whole lysimeter volume this yields a concentration of 0.08759 g/L. **Table 2** shows the exact g/g concentration for each lysimeter by taking the different bulk density and mass of the soil within the lysimeter into account.

Table 2. Microplastic input concentrations for field 1 and field 2.

Site	Average Pb [g/cm^3]	Soil Mass [g]	Concentration [g/g]
Field 1 (Till)	1.40945	16573.44159	0.0000621476
Field 2 (No-till)	1.533805	18035.70725	0.0000571089

2.3.3. Description of the MP infiltration

After spiking the lysimeters, Milli-Q water was poured over the soil surface to accelerate microplastic infiltration into the soil. The infiltration period was one week. After that, the field experiment started on August 28, 2023, and finished on February 12, 2024, resulting in an experiment duration of 5.5 months (168 days). The experimental design is given in **Figure 3**.

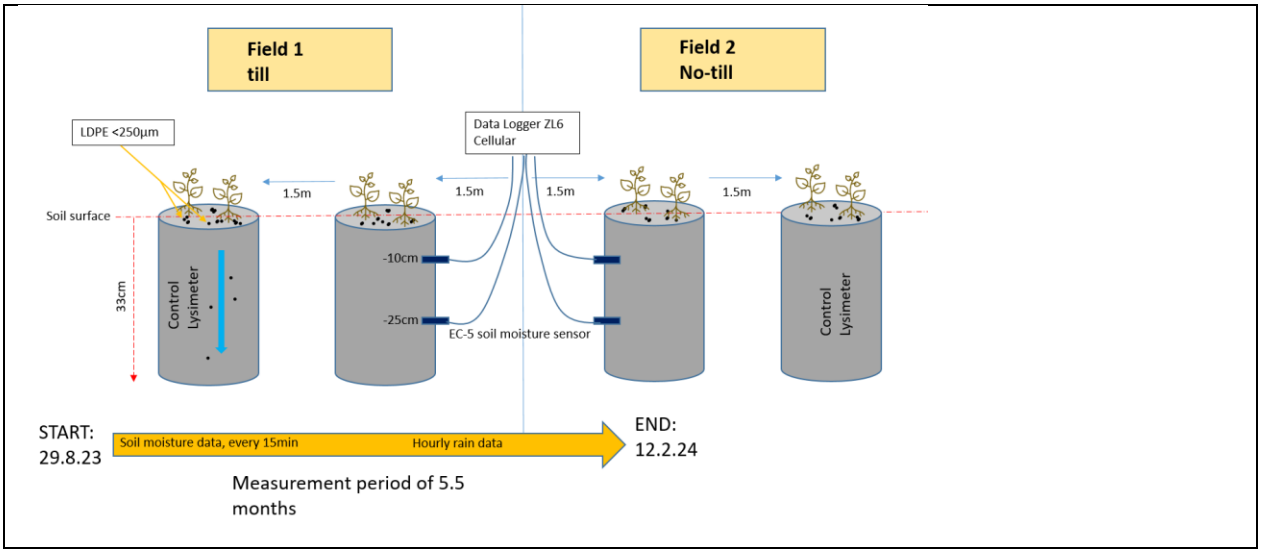

Figure 3. Overview of the experimental set up in Unterzollikofen (BE) (own work, 2024).

For the field experiment conducted in this study, four TDR soil moisture sensors ECH20 EC-5 from METER Group were used. The measurement range of the EC-5 in soil media ranges from 0 to 0.55 m^3/m^3 volumetric water content and has a resolution of 0.001 m^3/m^3. Calibration of these sensors was followed according to the METER Group recommended calibration guide (Method A) (Soil-specific Calibrations,

METER, n.d.). The calibration guide follows the general procedure for calibrating soil moisture sensors outlined by Starr and Paltineanu (2002). soil properties were analyzed at 10 cm and 25 cm depth in each field, which corresponds to the sensor installation depth. Soil properties analyzed in this study are bulk density, pH, soil texture, soil organic matter, saturated hydraulic conductivity (K_{sat}) and water retention (WRC). For bulk density, K_{sat} and water retention analysis, 250 ml steel cylinder sample rings were used. Bulk density analysis was performed immediately after sampling (more details are given in Ly, 2025).

2.3.4. Dye tracer experiments

A dye tracer experiment was conducted to additionally produce semi-quantitative data on soil structure and water flow of fields 1 and 2. The experiment was started on February 13, 2024 and ended on February 14, 2024. The water infiltration experiment was conducted approximately 2 m away from the lysimeter installation location. Brilliant blue was used as dye tracer with a concentration of 4 g/L. A total of 15.5 L of brilliant blue was infiltrated on an area of 1963.49 cm^2. The brilliant blue was distributed on the soil over a total time of 1 hour, simulating high-intensity rainfall of 80 mm/h. Irrigation was performed manually with the help of a water can. 24 hours after infiltration, two soil profiles were dug out and photographed in front of a 50x50 cm grid. The profiles were dug out at r = 25 cm of the circle-shaped area (**Figure 4**).

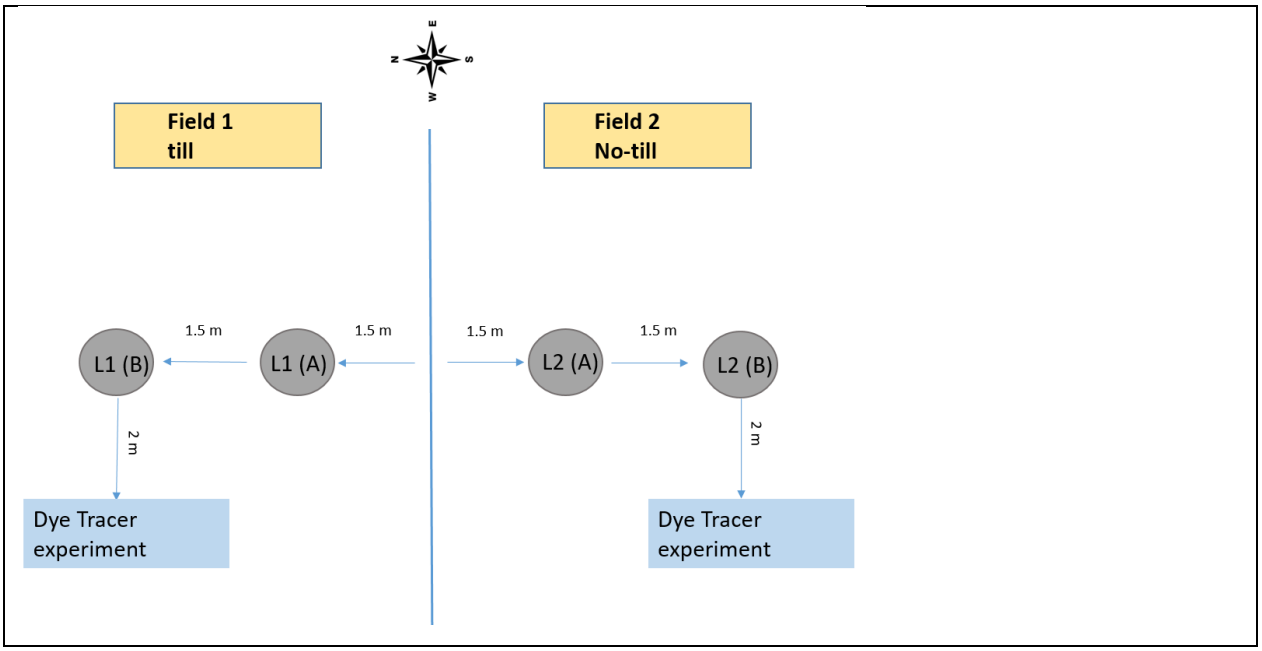

Figure 4. Sketch of the dye tracer location on the study field. L1 refers to lysimeter in field 1. L2 refers to lysimeter in field 2, respectively, A and B refer to control and spiked lysimeters, respectively.

2.3.5. Sampling design

After the measurement period, starting in August 2023, soil was sampled from the lysimeter on February 12, 2024. A sampling auger was used to sample soil from within the four lysimeters. For each lysimeter, four bore holes were made. Every 5 cm the soil was sampled with four drillings, mixed and stored in non-

plastic envelopes for transportation. The sampling depth goes 10 cm below the actual lysimeter depth, which was 35 cm, meaning that soil was sampled to a depth of 45 cm below the surface (**Figure 5**). Additionally, approximately 10 g of soil was scratched off the surface with a small spatula and stored in the same way. Apart from that, field-blank samples were taken the same way for field 1 and 2. The field-blank sampling was necessary to analyze the microplastic quantity of the non-spiked soil, so that an accurate particle estimation was possible by subtracting the blank quantity from the spiked soil. Therefore, the field-blank soil was sampled 5 m away from the lysimeters. The 5 m distance was chosen to minimize the risk of contamination of microplastic by wind dispersion from the lysimeter to the outside soil, while still being close enough to represent the microplastic concentration of the local soil, prior to the lysimeter installation.

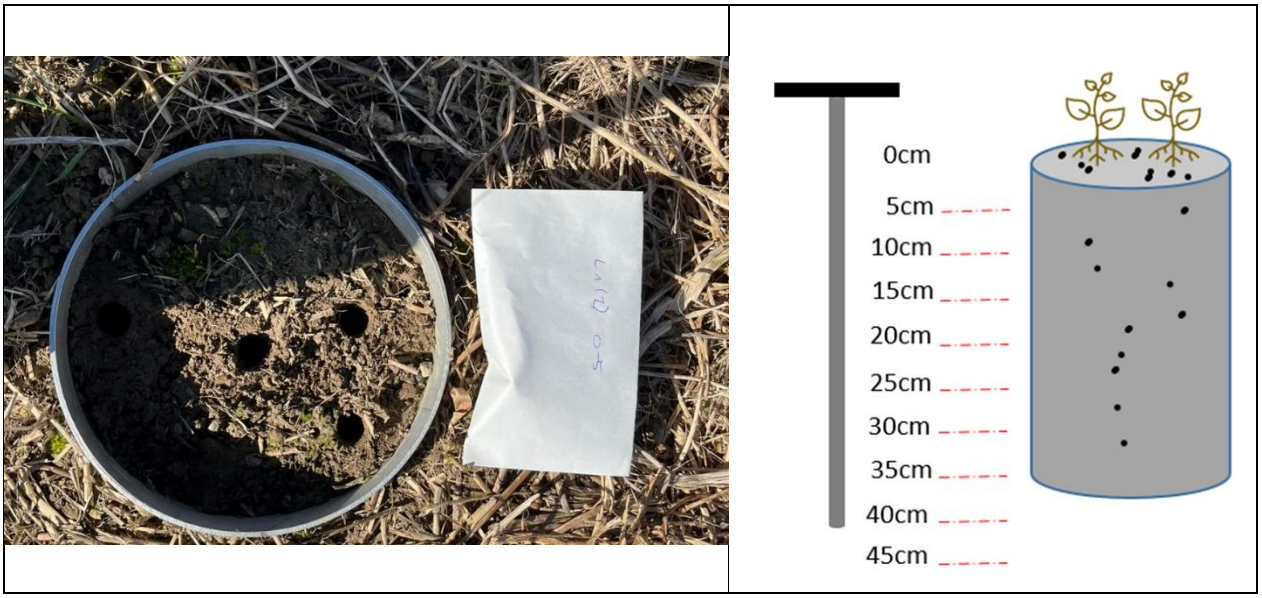

Figure 5. Aerial view of the lysimeter, showing 4 sampling bore holes, drilled with a sampling auger (taken on 13.12.2024).

The samples were analyzed in batches of 16 samples, including 15 soil samples and one blank sample. The whole extraction procedure was performed under a clean hood. The method of extraction is described in Tehrani et al. (2025) and Ly (2025).

3. RESULTS

Results are given by sections, following the order given in material and methods.

i) Experimental and modelling of MP in reconstructed soil columns

ii) Modelling MP transport in reconstructed soil under natural conditions

iii) Experimental and modelling MP in undisturbed soil under natural conditions

3.1. Experimental and modelling of MP in reconstructed soil columns

The soil hydraulic properties were determined using the evaporation method, and dispersity of soil columns was measured through a tracer experiment. The soil hydraulic properties are presented in **Table 3**, summarized as averages of three replications for both sandy loam soil and loamy sand soil. The residual water content (ϑ_r) was consistently set to 0.02, and the value of l was fixed at 0.5 for both soil types. The measured saturated water content (ϑ_s) was slightly higher for sandy loam soil (0.45) than for loamy sand soil (0.4). Fitted parameters, including the shape parameters α and n, along with the saturated hydraulic conductivity (K_S), varied between the soils. Loamy sand had a higher α value (0.08 cm^{-1}) and K_S 8 cm/h, suggesting different soil hydraulic functions. The R^2 values amounted to 0.9 and 0.91 for loamy sand and sandy loam soil, respectively, indicating a good fit for both soils. Additionally, the dispersivity, presented in **Table 3**, differed between the two soil types, with sandy loam showing a dispersivity of 1.2 cm and loamy sand with a dispersivity of 0.8 cm. These dispersivity values indicate variation in solute spread within each soil type, which could significantly impact microplastic transport behavior in subsequent experiments.

Table 3. Optimization of VGM parameters for each soil type using the evaporation method, and dispersivity values using tracer experiments.

Soil type	ϑ_r (-)	ϑ_s (-)	α (cm^{-1})	n (-)	k_s (cm/h)	l (-)	Dispersivity (cm)
Loamy sand	0.02	0.40	0.08	1.7	8	0.5	0.8
Sandy loam	0.02	0.45	0.04	1.6	6	0.5	1.2

Note: ϑ_r [-] is the residual volumetric water content, ϑ_s [-] is saturated volumetric water content, α [cm^{-1}] is related to the inverse of the air entry pressure, n [-] is a measure of the pore size distribution, k_s [cm/h] is saturated hydraulic conductivity, and l [-] is an empirical parameter.

Figure 6 shows the observed and simulated release of microplastics during two imbibition and drainage cycles, along with water content probe data at 12 cm depth represented as gray line graphs. The measured data in these graphs is the average value of three replicates of each treatment. We used these average values as input data for inverse modelling. The initial retention of colloids occurred on the grain surface and at the interfaces when the bottom boundary condition was connected to a pressure of -100 cm water, and the water flux at the top was set to 0. The release was induced during imbibition when the water flux changed from 0 to 35 mm/h or 22 mm/h at the column top. Particles with weak adhesive forces will be

easily removed during the first drainage cycle and imbibition. In contrast, particles with stronger adhesive forces will be removed less efficiently in later cycles due to their stronger attachment to the soil.

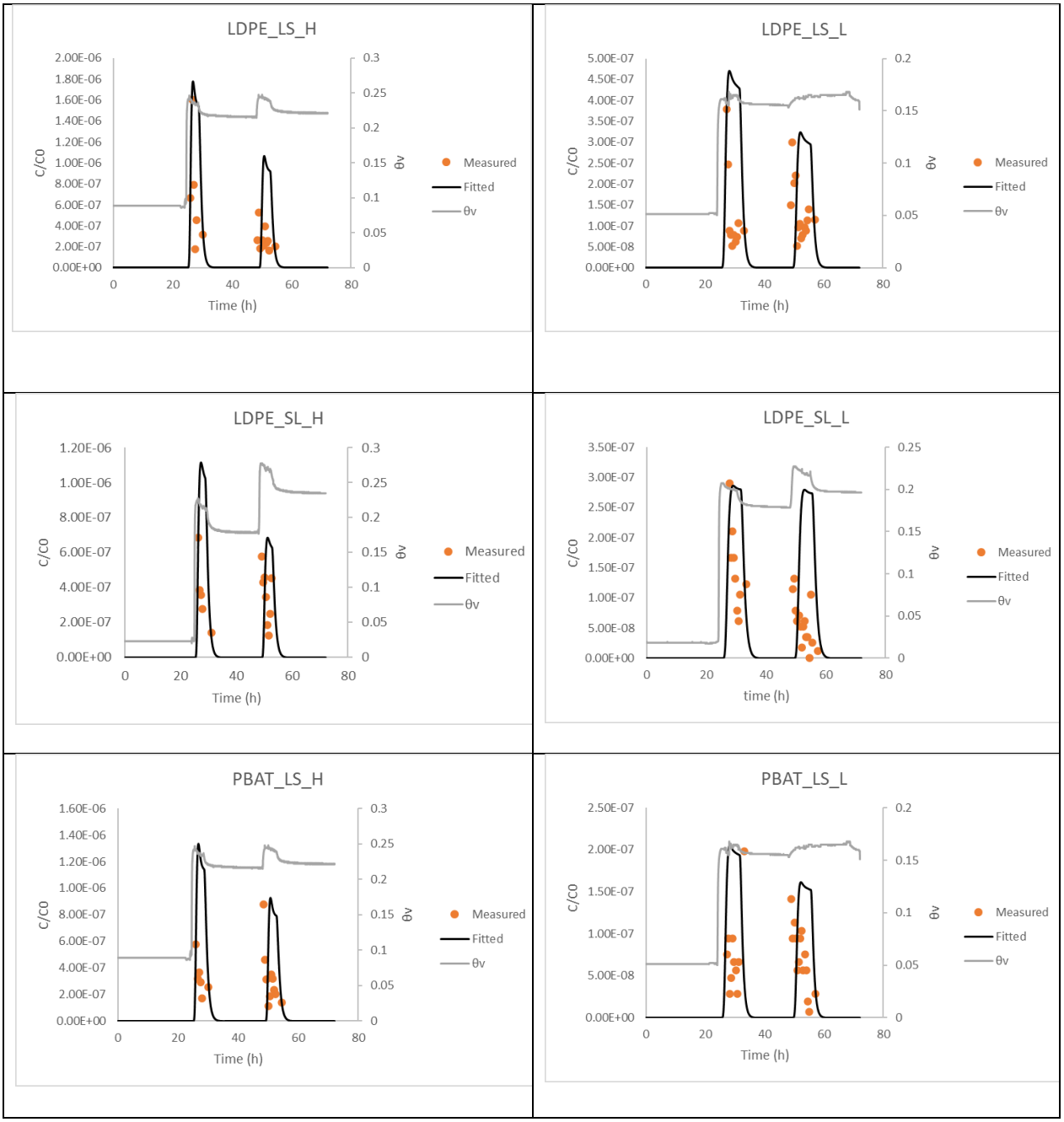

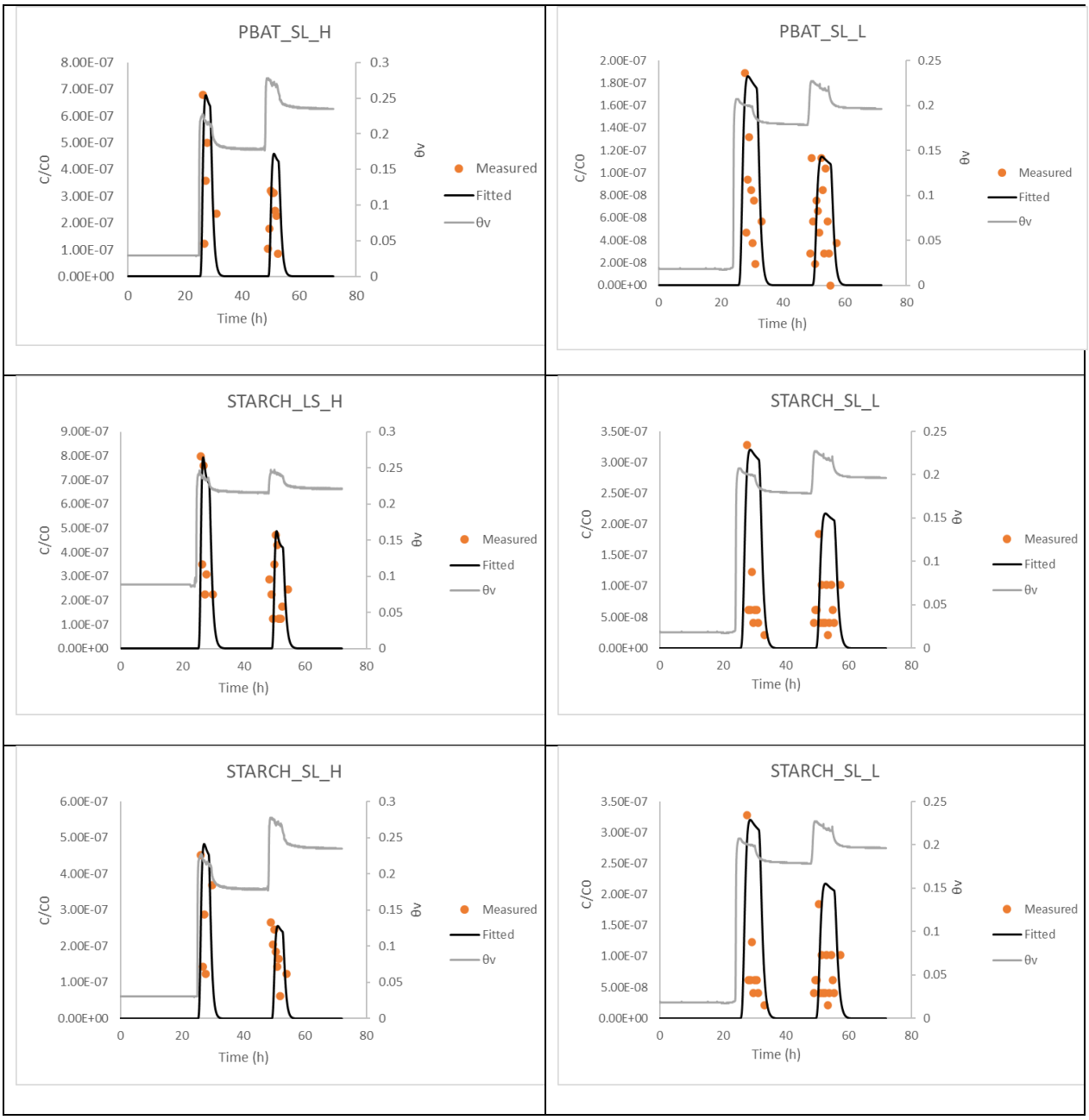

Figure 6. Observed and simulated breakthrough curves for different treatments. LS = loamy sand, SL = sandy loam, H = high rainfall intensity (35 mm/h), and L = low rainfall intensity (22 mm/h).

Notes: Observed data points are shown as orange circles and the model predictions as black lines. Gray lines show the water content probe data.

The two peaks in the breakthrough curves are related to the two rainfall events that were applied on the top boundary condition of the columns. In the sandy loam soil columns for all of the microplastics types and for both 35 mm/h and 22 mm/h rainfall intensity, the release of microplastics during the first rainfall event is higher than the second rainfall event. This difference can be attributed to the initial drier conditions during the first rainfall event compared to the second. In these drier conditions, particles tend to attach to surfaces and interfaces due to electrostatic forces (Wang et al., 2020). When water is added

during the first event, the redistribution of the electrostatic forces allows the particles to be released more easily. In contrast, during the second rainfall event, the porous media contains more water from the first event, and particles experience stronger electrostatic forces at the surfaces and interfaces, making it harder for them to be released. This is also observed in the loamy sand column except for the column spiked with PBAT under 35 mm/h rainfall intensity. The possible reason for this could be the transfer of particles to deeper layers, leading to accumulation and release during the next rainfall event. Initially, microplastics in the top 10 cm of the soil column were attached to soil surfaces. Due to soil water flow, shear forces redistribute MP at attachment points, releasing MP particles into the water and transporting them to larger depths. Depending on their size and surface characteristics, some particles may travel the full column length and enter the drainage water. During the second rainfall event, the entire column contains microplastics, so both remaining and previously transported particles can be released into the drainage water. The last sample after each rainfall event was collected 24 hours after the rainfall event. For the inverse modeling, the 24-hour data points were placed two hours after the previous data point.

The fitted BTCs are represented by the black line in **Figure 6**. The overestimation of peaks in some treatments, such as LDPE under low-intensity rainfall in sandy loam soil, could be caused by a combination of factors related to model assumptions and unique soil-microplastic interactions. The non-equilibrium model used in Hydrus-1D assumes one kinetic site, which may not fully capture the complex, transient retention and release dynamics for LDPE microplastics.

Comparing treatments, soil type had a notable effect, with loamy sand soil showing higher breakthrough concentrations for all microplastic types than sandy loam soil, indicating more efficient transport in coarser-textured soil. Rainfall intensity also played a key role, with higher intensity generally increasing breakthrough concentrations across all microplastics, especially for LDPE, which appeared to be more mobile under intense water flow. Under transient flow conditions, the hydrodynamic shear force is the dominant force during imbibition (Cheng and Saiers, 2010) and more colloids are mobilized by a higher flow rate (Shang et al., 2009). Differences between microplastic types were evident: LDPE showed the highest mobility likely due to its less complex surface properties, while PBAT showed moderate mobility and starch-based microplastics exhibited less mobility compared to the two other microplastics. The bigger breakthrough curve for LDPE is also related to the lower bulk density for this polymer compared to the other two polymers. The weight of added microplastics in all treatments is the same, and because of the lower density of LDPE, this polymer has more particles compared to the other two polymers, which can cause more transported particles. Overall, the Hydrus-1D model provided a good fit for the observed BTCs, effectively capturing the distinct transport pattern across soil types, rainfall intensities, and microplastic types.

The retention profiles in **Figure 7** show both observed (mean of 3 replicas) and fitted data for each treatment. Both data sets are related to the end of the experiment (72 h). Most graphs reveal that the fitted profile closely aligns with the observed data in the top 10 cm but deviates as depth increases. This trend suggests that while the model accurately represents retention processes at shallow depths, it encounters challenges in fully capturing dynamics influencing particle movement and retention at deeper depths. These deviations indicate potential deficiencies in the model concepts or parameters for these treatment conditions. In our inverse modelling approach, which incorporated both measured breakthrough curves and retention profiles as input data, adding a second kinetic sorption site did not

yield better BTC and retention fits. We suspect this may be due to the particle size of the microplastics used (< 250 µm, with the smallest particle size being 10 µm), as particle behavior in porous media heavily depends on particle size. This likely made it challenging for the model to capture the interactions between particles of varying sizes and the soil particles.

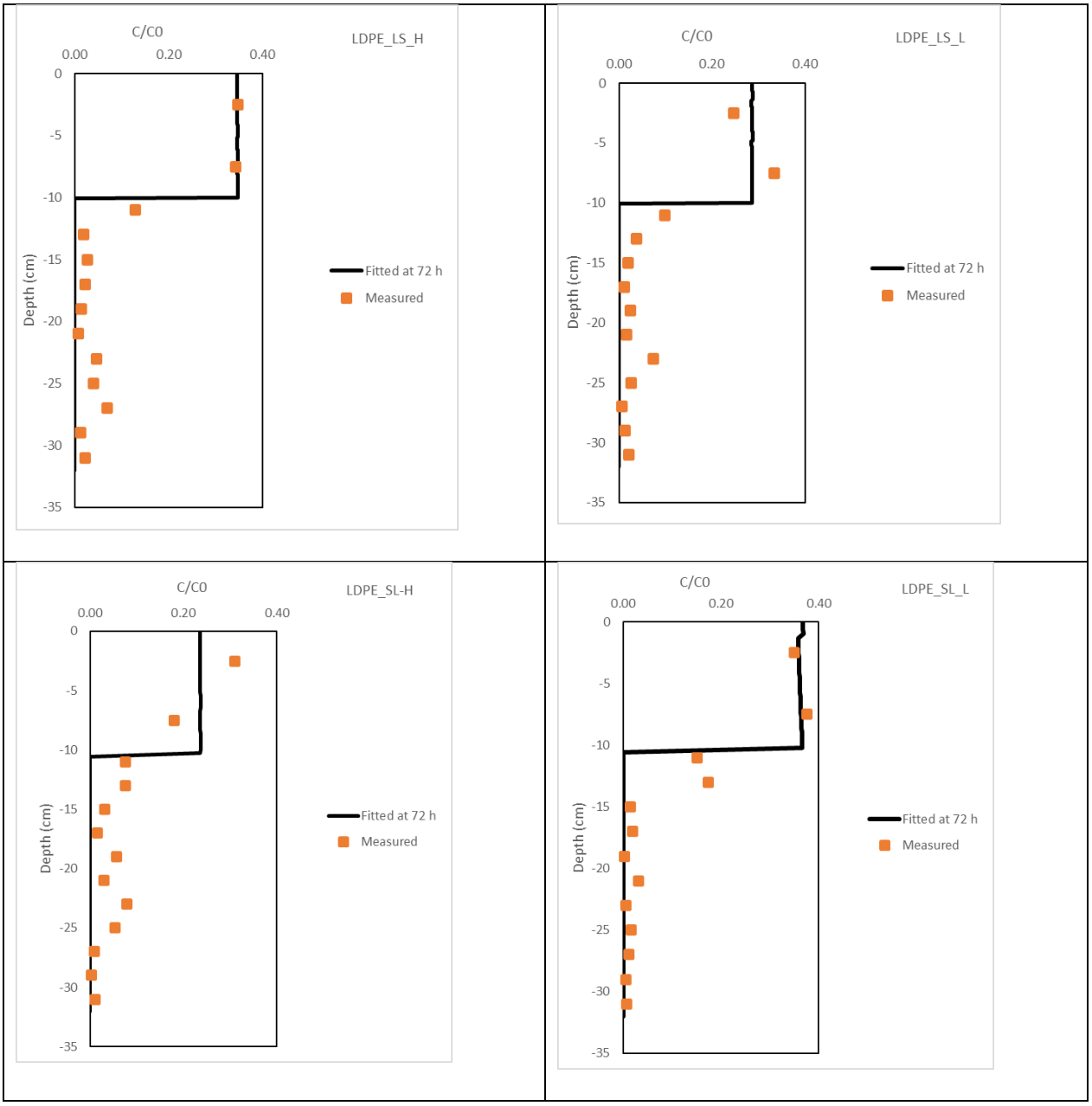

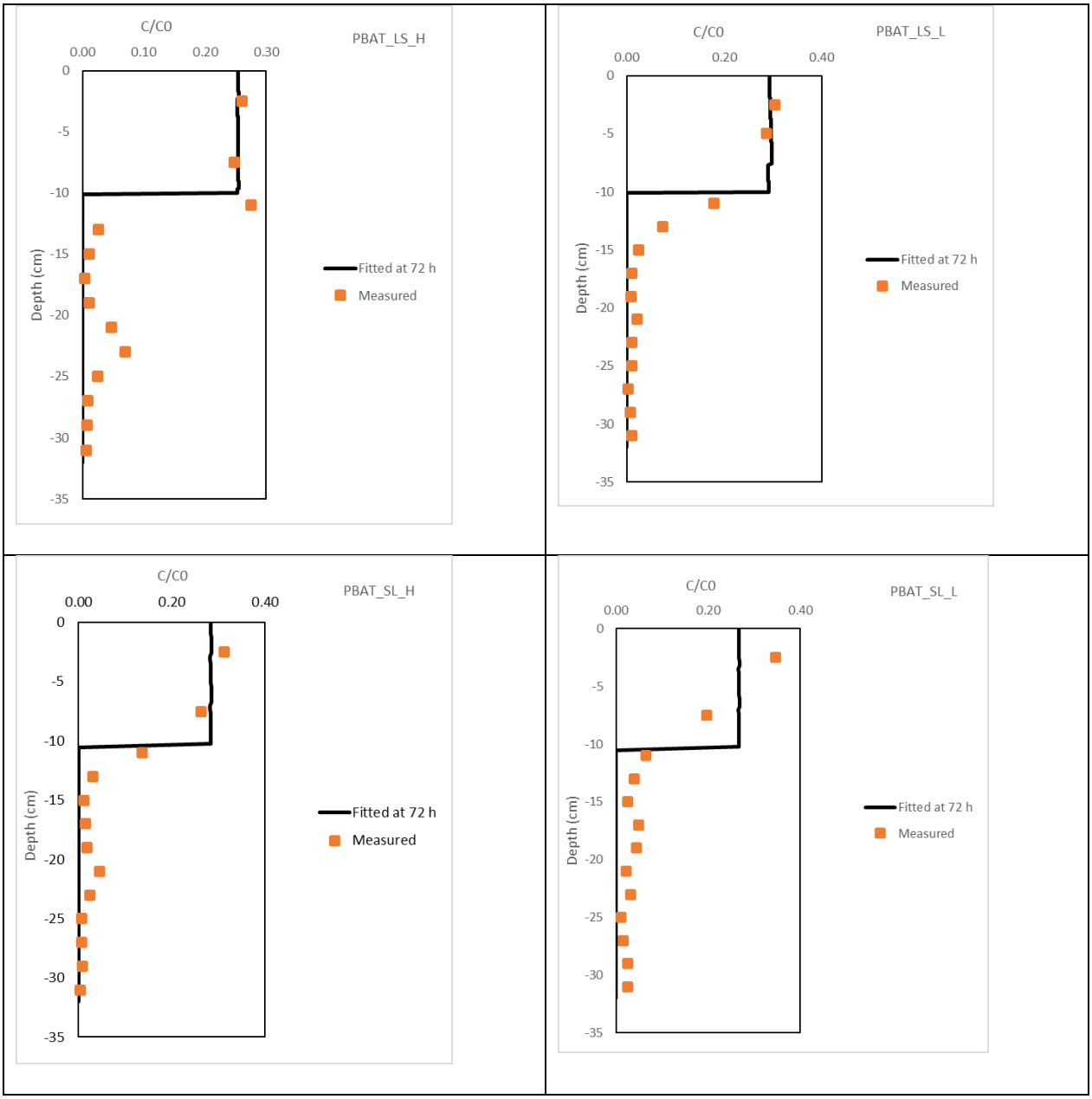
C/C0
PBAT_LS_H
0.00
0.10
0.20
0.30
0
-5
-10
-15
-20
-25
-30
-35
Depth (cm)
Fitted at 72 h
Measured
C/C0
PBAT_LS_L
0.00
0.20
0.40
Depth (cm)
Fitted at 72 h
Measured
C/C0
PBAT_SL_H
0.00
0.20
0.40
Depth (cm)
Fitted at 72 h
Measured
C/C0
PBAT_SL_L
0.00
0.20
0.40
Depth (cm)
Fitted at 72 h
Measured

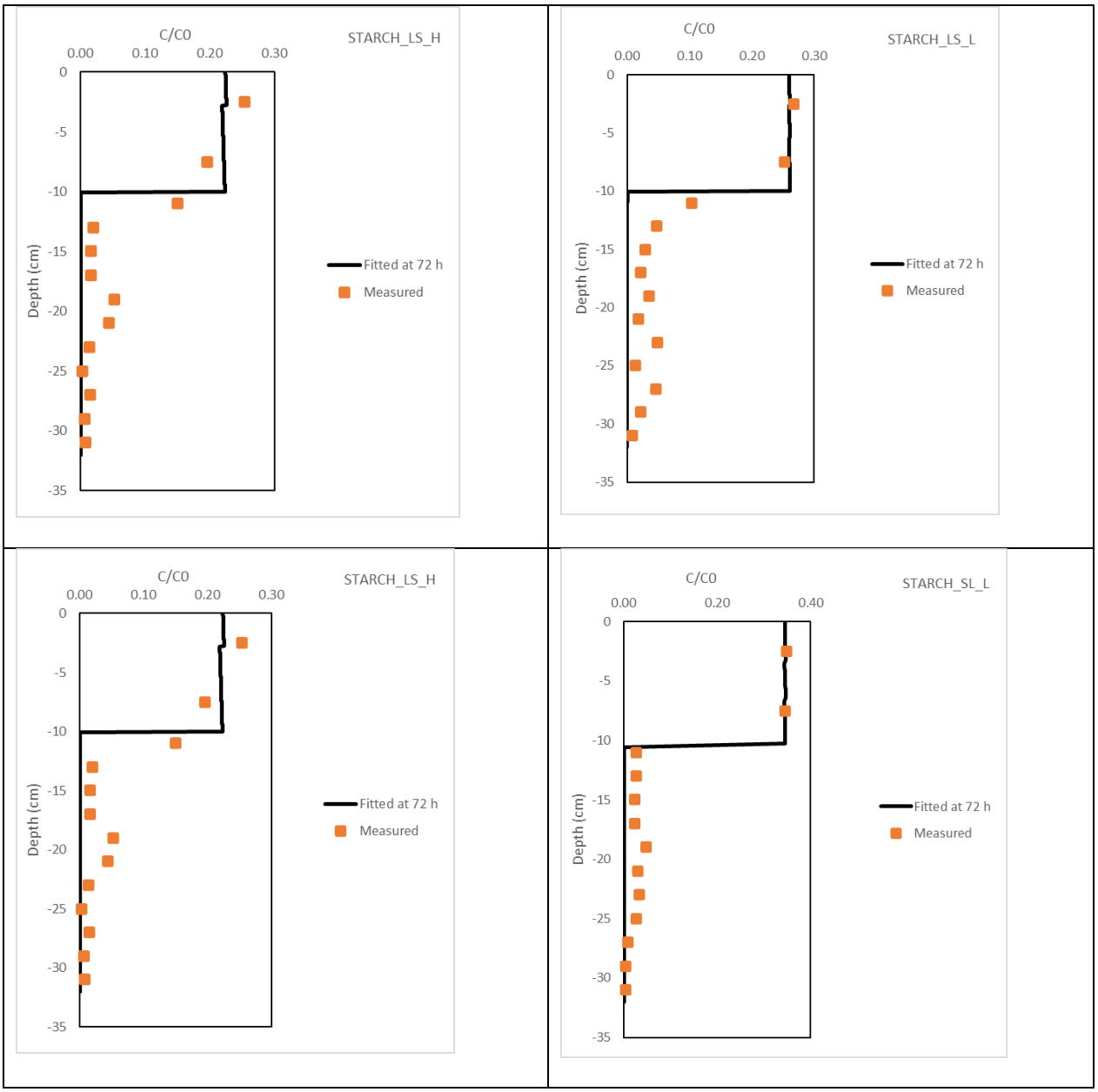

Figure 7. Observed and simulated retention profile for all treatments. LS = loamy sand, SL = sandy loam, H = high rainfall intensity (35 mm/h), and L = low rainfall intensity (22 mm/h)

Notes: Observed data points are shown as orange squares and the model predictions as black lines.

Table 4 presents the fitted parameters obtained from inverse modelling for various treatments. Key parameters are the β coefficient, which describes the shape of the retention profile (Eq. 4.8), and K_{att}, which represents the attachment rate to the kinetic site. The β coefficient varies between treatments, ranging from approximately 0.95 to 1.10, reflecting differences in retention profile shapes across soils and microplastic types. A β value close to 1 generally suggests a uniform retention profile shape, while a deviation from 1 indicates changes in particle distribution due to soil and plastic interactions.

Table 4. Fitted model parameters.

Treatment	β	K_{att}	R^2
LDPE_LS_H	1.10	1.49	0.90
LDPE_LS_L	1.03	1.36	0.88
LDPE_SL_H	1.04	1.32	0.78
LDPE_SL_L	0.95	1.23	0.82
PBAT_LS_H	1.01	1.36	0.60
PBAT_LS_L	0.99	1.55	0.82
PBAT_SL_H	1.03	1.52	0.87
PBAT_SL_L	1.06	1.55	0.85
STARCH_LS_H	0.96	1.36	0.77
STARCH_LS_L	1.07	1.53	0.87
STARCH_SL_H	1.10	1.77	0.76
STARCH_SL_L	1.05	1.40	0.97

Note: K_{att} [min^{-1}] is the first-order attachment coefficient, β [-] is an empirical variable that controls the shape of the retention profile, and R^2 reflects the correlation of observed and fitted data.

The attachment rate coefficient exhibits variation across treatments, with values ranging from approximately 1.23 to 1.77. Higher K_{att} values indicate stronger particle attachment to soil particles, which could be influenced by soil texture and microplastic type. For instance, treatments with starch-based microplastics in sandy loam soil under 35 mm/h rainfall intensity have a higher K_{att} value (1.77) than other treatments, which aligns with starch's biodegradable nature and potentially higher interaction with soil particles. Conversely, LDPE treatments, especially in sandy loam soil columns under 22 mm/h rainfall intensity have lower K_{att} values, suggesting lower attachment rates and possibly more mobility within the soil column. The R^2 values reflect the goodness-of-fit for each treatment with most values above 0.75, indicating reasonable model performance. Overall, these parameter variations provide insight into how soil texture and microplastic type influence retention and transport dynamics, underscoring the importance of tailoring model parameters to specific soil-microplastic interactions.

3.2. Modelling MP transport in reconstructed soil under natural conditions (Experiment I, Wageningen University).

Figure 8 presents the measured and fitted retention profiles for all treatments. The retention profiles of the spiked microplastics, including LDPE, PBAT, and Starch-based, show distinct temporal and spatial behaviors within the soil columns. The initial spiking of the top 10 cm with the respective plastic types resulted in observable retention patterns that evolved over the 6-month and 12-month collection periods.

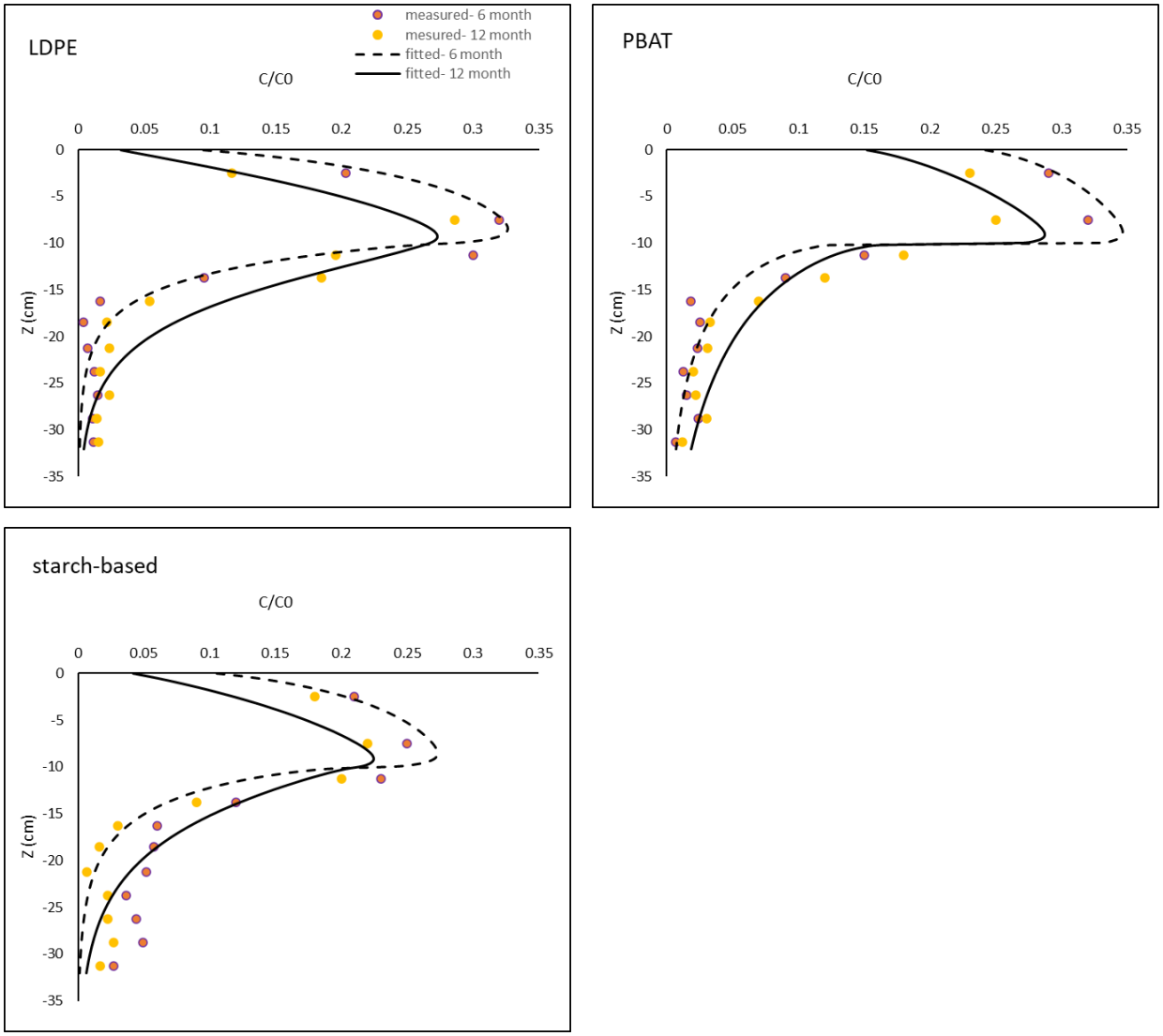

Figure 8. Observed and simulated retention profile for all treatments, averaged across replicates

For LDPE treatment, the retention profiles (C/C0) exhibited relatively consistent distribution across soil depths at 6 months, with a gradual decline in concentration at larger soil depths. However, after 12 months, a notable decrease in retention was observed at shallow depths (0 to 10 cm), coupled with a slight increase at greater depths, suggesting downward migration processes increasing the plastic residue.

The PBAT treatment demonstrated similar trends, with retention values showing a more uniform distribution across the soil profile at 6 months than LDPE. At 12 months, a slight convergence of the retention profiles at lower depths (10 to 32 cm) was evident, possibly indicating more efficient degradation or dispersal of PBAT relative to LDPE over time.

The starch-based treatment showed the most pronounced changes between the two collection periods. At 6 months, the retention values were concentrated near the top 10 cm, with a sharp decline more profound at larger depths. By 12 months, retention values were significantly reduced at shallow depths and distributed more evenly across the profile, particularly in the lower soil depths. This suggests a higher rate of degradation compared to the other treatments.

The HYDRUS modeling results provided insights into the retention of LDPE, PBAT, and starch-based within the soil columns in the field. The model successfully fitted the retention profiles to the measured data, with high R^2 values ranging from 0.83 to 0.95, indicating a good agreement between observed and simulated results (**Table 5**). The optimized parameters, including the empirical retention profile shape parameter (β), attachment rate coefficient (K_{att}), and detachment rate coefficient (K_{det}), revealed distinct temporal and material-specific patterns. Additionally, degradation parameters (λ_L and λ_S) were included for PBAT and starch-based microplastics to account for their biodegradability.

Table 5. Fitted model parameters after field experiment I.

Treatment	β	K_{att}	K_{det}	λ_L	λ_S	R^2
LDPE	8.34E-01	1.81E+00	2.24E-02	-	-	0.91
PBAT	8.58E-01	2.88E-01	3.98E-03	2.05E-05	9.09E-05	0.95
Starch-based	8.01E-01	1.10E+00	1.39E-02	1.80E-03	3.08E-05	0.83

Note: K_{att} (day^{-1}) is the first-order attachment coefficient, K_{det} (day^{-1}) is the first-order detachment coefficient, β [-] is an empirical variable that controls the shape of the retention profile, λ_L is first-order degradation in the liquid phase, λ_S is first-order degradation rate in the solid phase, and R^2 reflects the correlation of observed and fitted data.

For LDPE, the optimized β parameter (0.834) suggests a consistent retention profile shape across both time points. The attachment rate coefficient of 1.81 day^{-1} indicates strong particle-soil interactions, leading to significant immobilization of LDPE in the soil matrix. The detachment rate coefficient of 0.0224 day^{-1} suggests limited but persistent remobilization. Unlike PBAT and starch-based microplastics, no degradation terms were included for LDPE, confirming its stability and negligible transformation within the soil over 12 months.

For PBAT, the β parameter (0.858) indicates a sharper decline in concentration with depth compared to LDPE. The attachment rate coefficient of 0.288 day^{-1} is lower than that of LDPE, suggesting weaker interactions with the soil matrix, possibly due to PBAT's partial biodegradability. The detachment rate coefficient of 0.00398 day^{-1} is significantly lower than that of LDPE, indicating that PBAT particles are less likely to be remobilized once retained. The inclusion of degradation parameters suggests that PBAT undergoes measurable transformation over time, contributing to its gradual reduction in retention at later stages. For starch-based microplastics, the β parameter (0.801) suggests a more gradual decline in concentration with depth compared to PBAT and LDPE. The attachment rate coefficient of 1.10 day^{-1} is

lower than LDPE but higher than PBAT, reflecting moderate particle-soil interactions. The detachment rate coefficient of 0.0139 day^{-1} is slightly higher than that of PBAT, indicating a greater tendency for remobilization. Notably, starch-based microplastics exhibited the highest degradation rate ($\lambda_L = 1.80 \times 10^{-3}$ day^{-1} and $\lambda_S = 3.08 \times 10^{-5}$ day^{-1}), confirming their substantial breakdown within the soil over time. This aligns with the observed reduction in retention, particularly near the inlet, suggesting active degradation-driven removal.

Overall, the modeling results highlight distinct behavior for the three microplastic types. LDPE exhibited stable retention dynamics over time, with limited changes in the retention profile. In contrast, PBAT and starch-based showed significant temporal shifts in their parameters, corresponding to the distribution of particle size in the soil and probably the onset of their biodegradability and transformation in the soil environment.

3.3. Experimental and modelling MP in undisturbed soil under natural conditions (Experiment II. Switzerland).

An overview of the determined soil properties is provided below. The data is summarized as average values for the respective soil properties by location. Standard deviation and detailed results are provided in the sections below.

3.3.1. Laboratory results

Basic soil parameters are given in **Table 6**. Soil ranges from loam to sandy loam with BD increasing in Field 3.

Table 6. Overview of the soil properties in field 1 (till) and 2 (no-till).

Location	Clay (%)	Silt (%)	Sand (%)	Texture	BD (g/cm³)	OM (%)	TOC (%)	pH
Field 1 10cm	10.57	41.46	47.76	loam	1.33	4.8	1.47	4.58
Field 1 25cm	8.4	36.18	55.4	sandy loam	1.48	4.71	1.42	4.69
Field 2 10cm	10.72	42.53	46.73	loam	1.53	4.31	1.33	4.13
Field 2 25cm	12.57	43.52	43.9	loam	1.53	4.16	1.1	4.9

Texture taxonomy according to USDA; BD: bulk density

The K_{sat} values show a high deviation among the duplicates of field 1 at 25 cm, field 2 at 10 cm and field 2 at 25 cm (**Table 7**). The deviation from the average value from these three locations ranges from 123% in field 2 at 10 cm to 134% in field 1 at 25 cm. The deviation in field 1 10 cm is lower at only 11% from the average value.

Table 7. Detailed overview of Ksat results, showing number of samples and standard deviation for field 1 (till) and field 2 (no-till).

Location	**Sample 1** [mm/h]	**Sample 2** [mm/h]	**Average Ksat** [mm/h]	Standard Deviation
Field 1 10 cm	221.46	189.44	205.45	11.02
Field 1 25 cm	16.39	611.11	313.75	134.03
Field 2 10 cm	537.50	7806.94	4172.22	123.20
Field 2 25 cm	800.00	71.11	435.56	118.33

The retention parameters are provided in **Table 8**, where alpha = parameter related to the inverse of the air entry section, n = shape parameter related to pore-size distribution, θ_r = residual water content (volumetric) and θ_s = saturated water content. The shape parameter m used in the Van Genuchten model used in this study is expressed as m=1−1n (Van Genuchten 1980).

Table 8. Overview of the retrieved Van Genuchten parameters for field 1 (till) and field 2 (no till).

Location	alpha 1/cm	N	θ_r (cm³/cm³)	θ_s (cm³/cm³)
Field 1 10cm	0.0554	1.17	0.074	0.421
Field 1 25cm	0.1121	1.336	0.153	0.442
Field 2 10cm	0.1751	1.122	0	0.453
Field 2 25cm	0.1992	1.144	0.028	0.411

θ_r: Residual water content; θ_r: saturated water content

3.3.2. Meteorological data

Hourly rain data was collected from the weather station from MeteoSchweiz in Zollikofen (MeteoSchweiz, 2024), 250 m away from the study location (see **Figure 2**). Soil moisture data was collected over a period of five and half months (168 days) (**Figure 9**). Prior to the start of the field experiment, the rain data shows a maximum hourly average of 5.4 mm/h on August 26, 2023. After that a dry phase of approximately one month occurred with no significant rainfall. In September several light to moderate rainfall events happened, with the soil moisture values slowly declining after precipitation occurrence. The highest rainfall intensity recorded during the investigation period was 9.7 mm/h in October. From October to February the climate became more wet, thus leading to an increase in soil moisture values. In field 1 upper and lower sensor values were similar. In field 2 the soil moisture was lower at 25 cm, than at 10 cm (**Figure 10**).

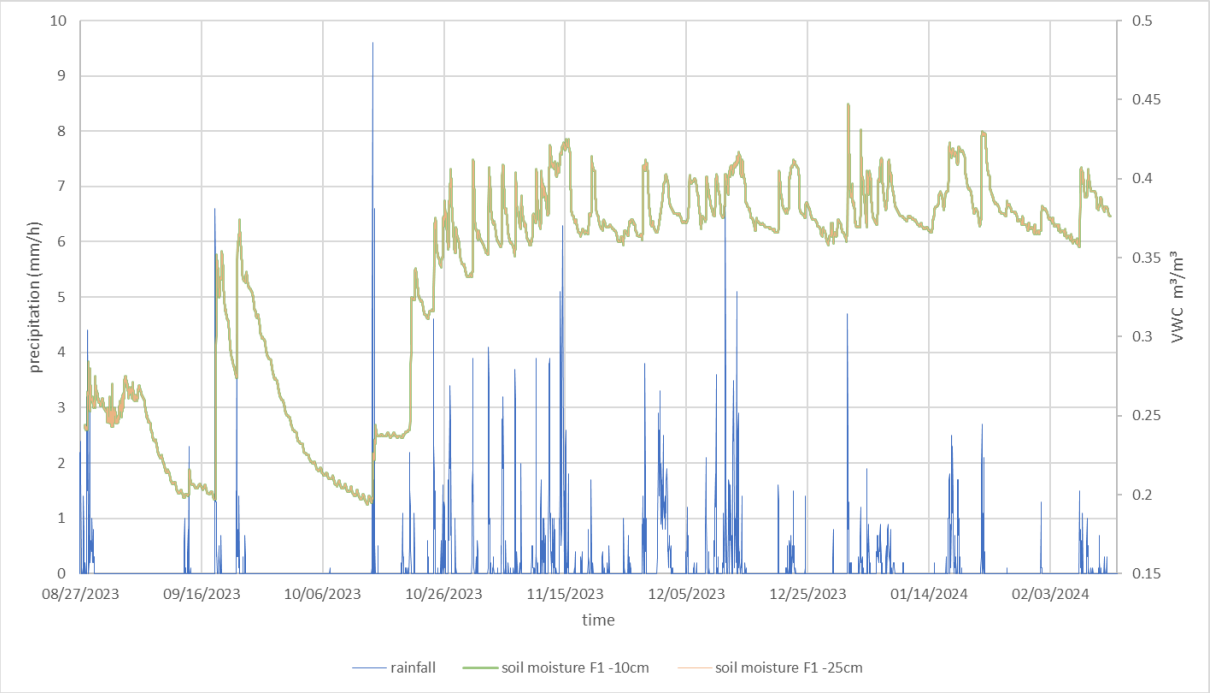

Figure 9. Observed and simulated retention profile for all treatments, averaged across replicates

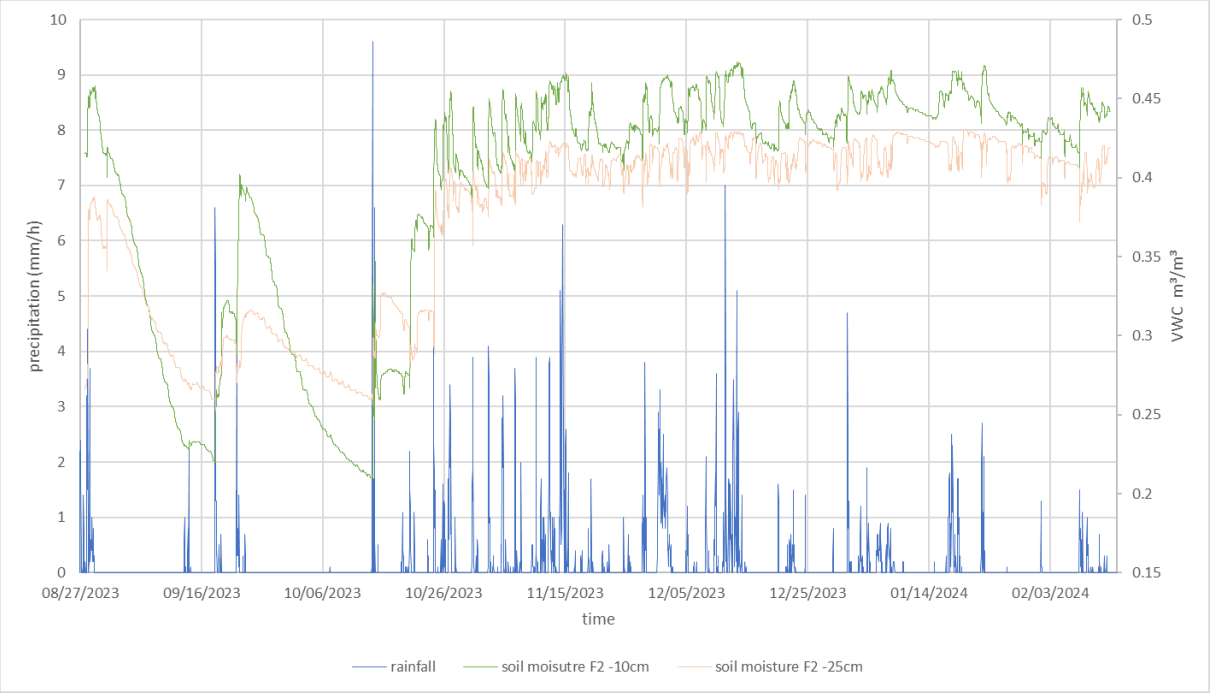

Figure 10. Rain and calibrated soil moisture data in field 2 (no-till)

3.3.3. Microplastic analysis

In advance it is important to note, that for microplastic analyses a referenced depth of 5 cm is associated with a depth range of 0-5 cm. Therefore, 10 cm means 5-10 cm respectively. The only exception to this rule is 0 cm which refers to the surface soil.

The following data provided below is blank corrected. For the blank correction two different sets of blanks were used. First, the number of particles and total area of the labour blank used during the extraction process were subtracted from the respective sample batches as well as from the field blanks. After this first blank correction, the results of the field blanks, which represent the already existing microplastic concentration in the soil before the experiment, were subtracted from the concentration found in each soil layer and field type. For better understanding, the microplastic concentration of the un-spiked soil was analyzed in an interval of 5 cm and then subtracted from the concentrations of the respective 5 cm layers found within the lysimeters.

Furthermore, the results were slightly adapted as described in section 2.5.4. Due to a methodological error a count correction was applied to the results. **Figure 11** shows the corrected microplastic concentration for lysimeter A in field 1 compared to the uncorrected data. The difference of both concentrations at 0 cm is 1485 particles/g. At 5 cm it goes down to a difference of 213 particles/g. At 15 cm the difference in concentration is only 23 particles/g and is getting smaller in the deeper layers of the soil. While the segmentation model determines the total number of particles to be 777 (particles/5g), the count correction produces a value of 8201 particles (particle/5g). This results in an increase of over 1000%, which is not surprising regarding the huge amount of microplastic visible on the filter. With depth, the number

of microplastics decreases, explaining the reduction in error. It is 106% between 0 and 5 cm and 34% between 10 and 15 cm. The significant difference between the estimates (corrected vs. uncorrected) can be explained by the fact that particles packed tightly together are not clearly differentiated and therefore not counted accurately (Foetisch et al., 2024).

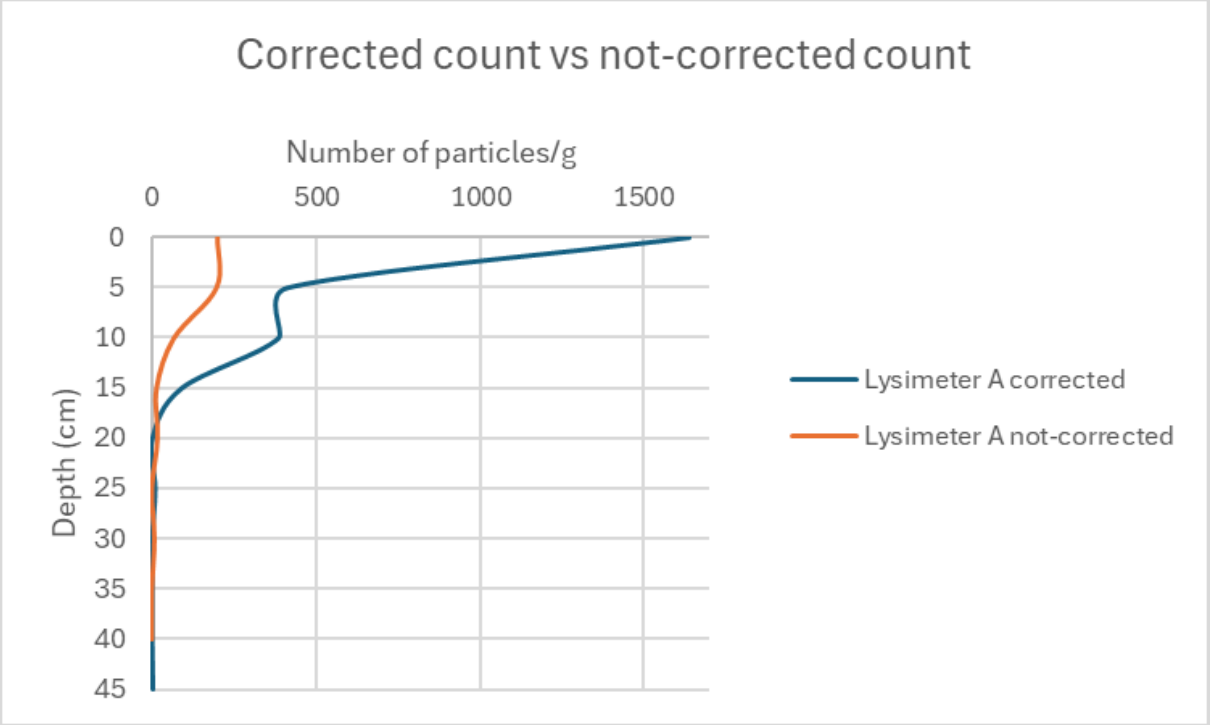

Figure 11. Graph showing the difference between the result for the uncorrected microplastic concentration values and the corrected values

The blank corrected and count corrected results for microplastic concentration in field 1 are provided below. In field 1 (till) the concentration found in the upper layers vary between lysimeter A and B (**Figure 12**). While the concentration at 0 cm in lysimeter A is 1640 particles/g, in lysimeter B the concentration found was lower at 789 particles/g. In lysimeter A a sharp decrease in concentration can be observed already at 5 cm depth. This concentration of 400 particles/g stays constant to 10 cm depth and abruptly drops to a concentration of less than 9 particles/g in deeper levels. Lysimeter B shows a constant, but sharp drop from 789 particles/g at 0 cm to 77 particles/g at 10 cm. No microplastic was found in both lysimeters from 30 cm to 40 cm depth. However, at 45 cm a concentration of 2 particles/g in lysimeter A and a concentration of 11 particles/g in lysimeter B was found.

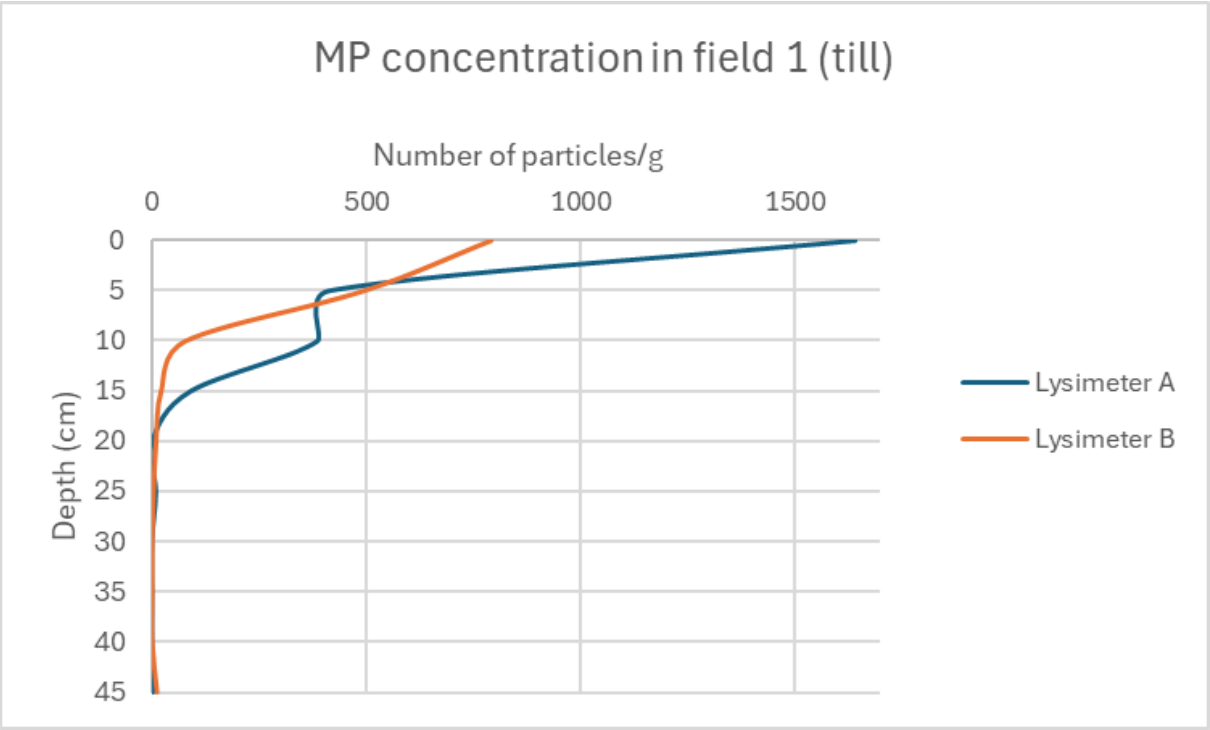

Figure 12. Results for microplastic concentration per depth in lysimeter A and B of field 1 (till) in particle/g

The results of the microplastic analysis for field 2 (no-till) are provided below in **Figure 13**. The deviation of the data from both lysimeters in field 2 is lower than in field 1. The concentration in lysimeter A at 0 cm is 382 particles/g and in lysimeter B the concentration amounts to 620 particles/g. The concentration decreases in both lysimeters to approximately 340 particles/g at 5 cm and continues to drop constantly to 25 particles/g at 15 cm in lysimeter A. In lysimeter B, the microplastic concentration amounts to 164 particles/g at 10 cm and increases again at 15 cm to a value of 217 particles/g. While the concentrations in lysimeter A stay constantly below 22 particles/g at deeper levels, the concentrations in lysimeter B fluctuate. After dropping to a concentration of 15 particles/g at 20 cm depth, the value rises again to 78 particle/g at 25 cm depth in lysimeter B, before dropping to 5 particles/g at 40 cm depth.

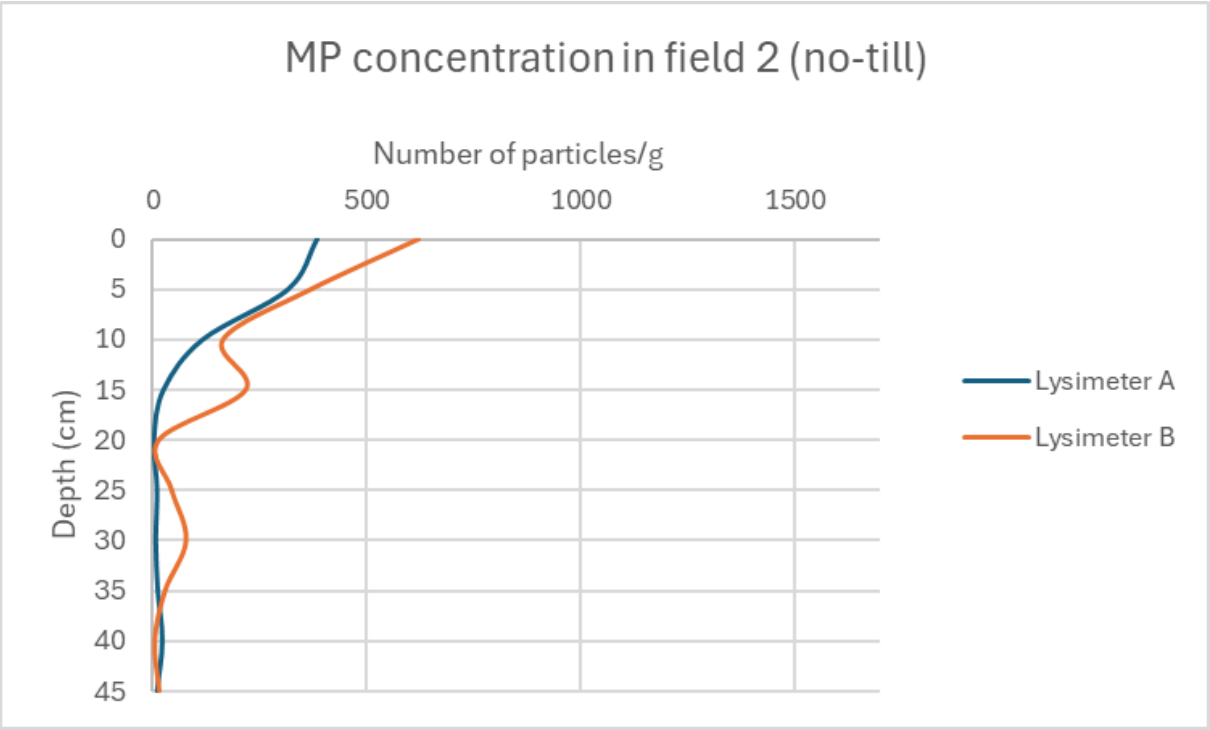

Figure 13. Results for microplastic concentration per depth in lysimeter A and B of field 2 (no-till) in particle/g

The following **Figure 14** provides the average concentration for field 1 and field 2. The values of lysimeters A and B for each field were used to calculate an average. The concentration in field 1 (till) in the first 15 cm is higher than the concentration in field 2. Below 15 cm, the average microplastic concentration in field 1 stays below 7 particles/g. The concentrations below 15 cm in field 2 fluctuate between 9 particles/g at 20 cm and a peak of 43 particles/g at 30 cm. Generally, the concentrations below 15 cm found in field 2 were higher than in field 1.

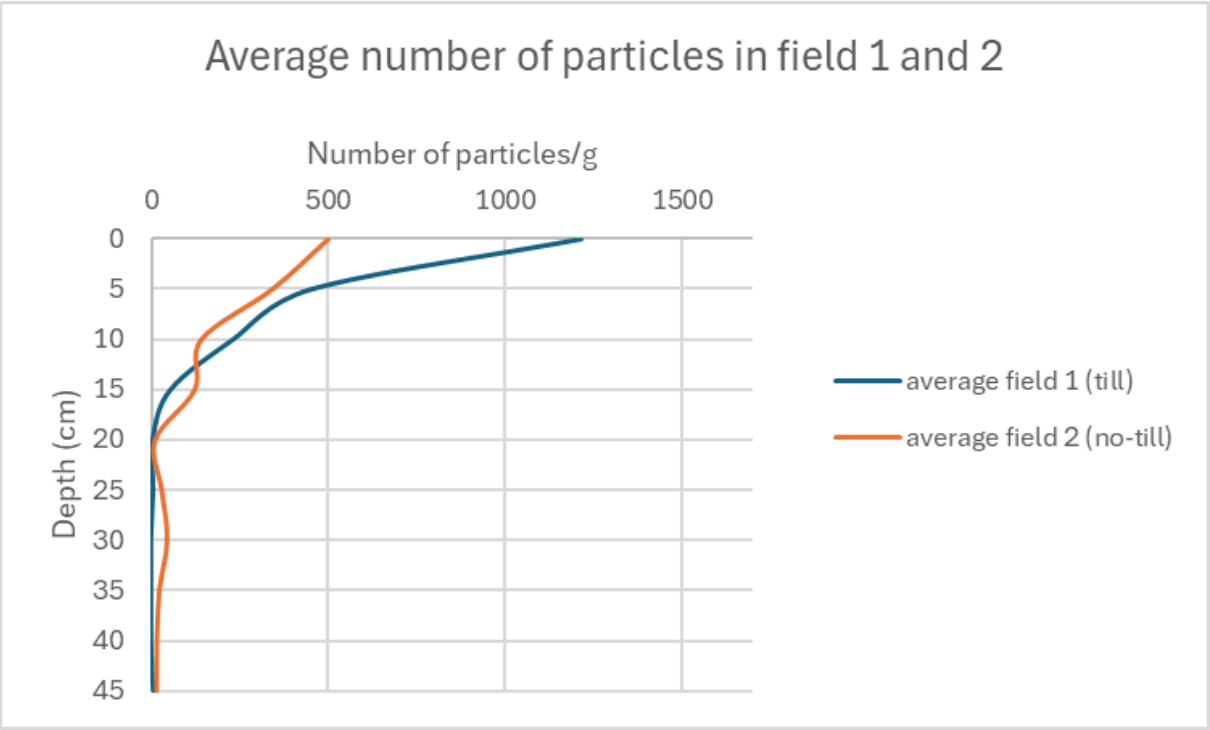

Figure 14. Calculated average concentration values per depth from lysimeters A and B of the respective fields

The average particle size was calculated with the help of an R-script and used for the count correction. The size distribution per depth for field 1 and 2 are provided in the figures below. Field 1 shows a clear downfall in particle size around 5-10 cm depth (**Figure 15**). The average particle size in field 1 continuously decreases between 10 cm and 20 cm depth. At 20 cm depth the average size stays the same. In field 2 an abrupt decrease in average particle size was detected at 10 cm depth (**Figure 16**). Below 15 cm depth the average particle size stopped continuously decreasing and remained approximately the same. The results from lysimeter A in field 2 show fluctuations in average particle sizes at deeper soil levels.

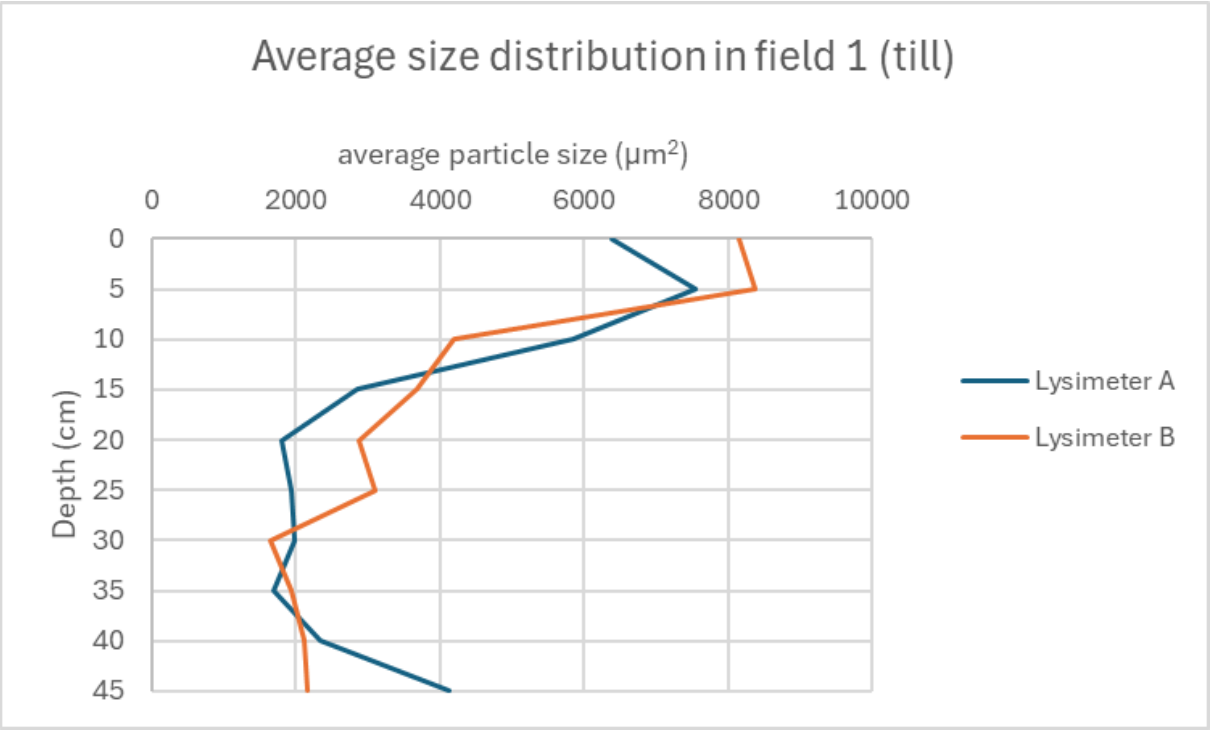

Figure 15. Average MP size distribution of lysimeters A and B of field 1 (till)

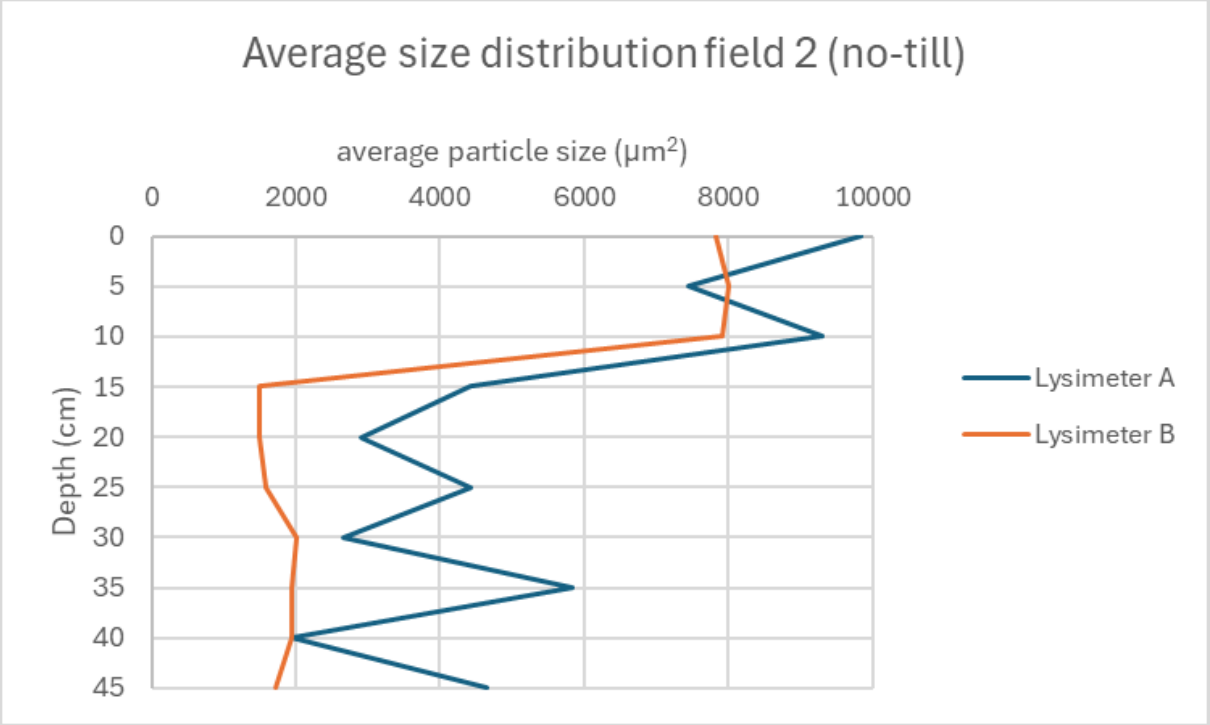

Figure 16. Average MP size distribution of lysimeter A and B of field 2 (no-till)

3.3.4. Dye tracer analysis

The dye tracer experiment produced additional insight in the soil structure the two fields. In field 1 (till) the plow sole just below 25 cm associated with the tillage practice before the year 2006 is clearly visible. The plow sole at 15 cm is less pronounced and not as developed. However, the plow sole at 15 cm can be identified in the bulk density values of field 1, where the upper soil has a bulk density of 1.33 g/cm3 and the soil below 25 cm has a value of 1.48 g/cm3. The soil in field 1 below 25 cm shows signs of compaction, decreasing the speed of infiltrating water. Field 1 shows less preferential flow paths than field 2. This is linked to an uniform pore distribution that facilitates diffusive water flow, which is attributed to soil plowing. Water flow in field 2 (no-till) is dominated by preferential flow. This can be observed by the spatially concentrated water flow in the soil profile (Alaoui et al., 2011). Preferential flow of infiltrating water bypasses most of the porous soil matrix, which is indicated in the soil profile of field 2 (no-till) (**Figure 17**). In the upper soil (0-7 cm) of both fields, water movement is characterized by diffusive flow. This is an indicator of compaction of the upper soil, effectively destroying macropores in the topsoil. However, with increasing depth, preferential flow paths in field 2 become more distinguishable, indicating an abundance of biopores (**Figure 17**). No-till systems have been associated with higher earthworm activity, further supporting this argument (Peigné et al., 2009; Crittenden et al., 2014; Chan, 2001; Dekemati et al., 2019).

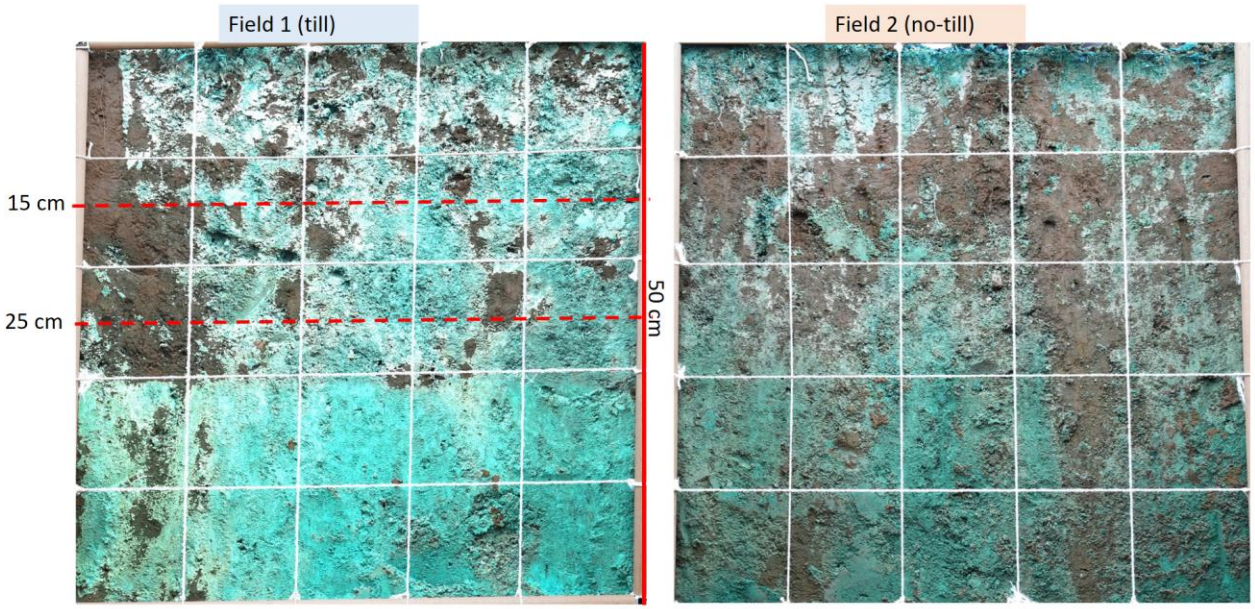

Figure 17. Processed images of soil profiles retrieved from the dye tracer experiment. The water colors are highlighted to accommodate visual interpretation

3.3.5. Earthworm activity

In the samples originating from field 2 several earthworm burrows were discovered, and one living earthworm was removed from the top of the sample (field 2 10 cm, sample 2). The samples from field 1 were less pierced by earthworm activity, thus showing fewer earthworm burrows than field 2. Earthworm activity can alter the soil structure and create more preferential flow paths. Several scientific studies (Peigné et al., 2009; Crittenden et al., 2014; Chan, 2001; Dekemati et al., 2019) argue that tillage practices significantly reduce earthworm populations. Chan (2001) states that tillage can change the abundance of

earthworms by 2-9 times as well as the diversity of earthworm populations. This aligns with the findings of this study regarding the area of earthworm burrows within the samples. Therefore, the permeability of the soil can be significantly increased due to earthworm activities, especially in field 2 (**Table 9**). Additionally, the dye tracer profile from field 2 showed that water is infiltrated mostly by preferential flow. **Figure 18** shows earthworm burrows.

Table 9. Ksat values affected by earthworm burrow (red), unaffected (green) and low impacted (orange).

Location	Sample 1 Ksat mm/h	Sample 2 Ksat mm/h	Bulk density g/cm^3	Soil type
Field 1 10cm	221.46	189.44	1.33	loam
Field 1 25cm	16.39	611.11	1.48	sandy loam
Field 2 10cm	537.50	7806.94	1.53	loam
Field 2 25cm	800.00	71.11	1.53	loam

According to the literature, the green colored numbers represent non-exaggerated values, while the red ones are largely overestimated values, due to a large amount of earthworm burrows (Alaoui et al., 2011). The orange-colored numbers also show high Ksat values, but are closer to typical Ksat values according to Clapp & Hornberger (1978), compared to the red numbers. However, the green Ksat value at field 1, 25 cm is not typical for sandy loam (125 mm/h). Since earthworm burrows were absent in this sample, the Ksat value of ? sample is therefore, lower in contrast to the other measurements. Since sample 2 from field 1, at 25 cm indicates a much higher Ksat value of the soil, than sample 1, this nicely outlines the effect of earthworm burrows on the soil permeability. However, the low Ksat value in field 1, at 25 cm can also be attributed to the effect of tillage practice used on this field. Through tillage of the upper soil, a distinct boundary between the loose, tilled soil and the soil below is created. This can form a dense layer, also known as the plow sole, impeding water infiltration due to reduced permeability and the absence of macropores. Furthermore, compaction of the soil is less likely, because the bulk density values do not show any sign of compaction of the soil. Bulk density of field 1, at 25 cm, field 2, at 10 cm and field 2, at 25 cm align with the typical densities attributed to their soil types. The bulk density value in field 1, 10 cm (**Table 6**) is below typical values for loam (**Annex 1**) thus suggesting a loosening of the soil. This nicely outlines the effect of tillage on the soil structure. Since tillage can significantly increase the permeability of the soil and only a small amount of earthworm burrows were detected within the soil samples for field 1 10 cm (orange), it can be concluded that the high permeability of the soil at the first 10 cm can be partly attributed to tillage.

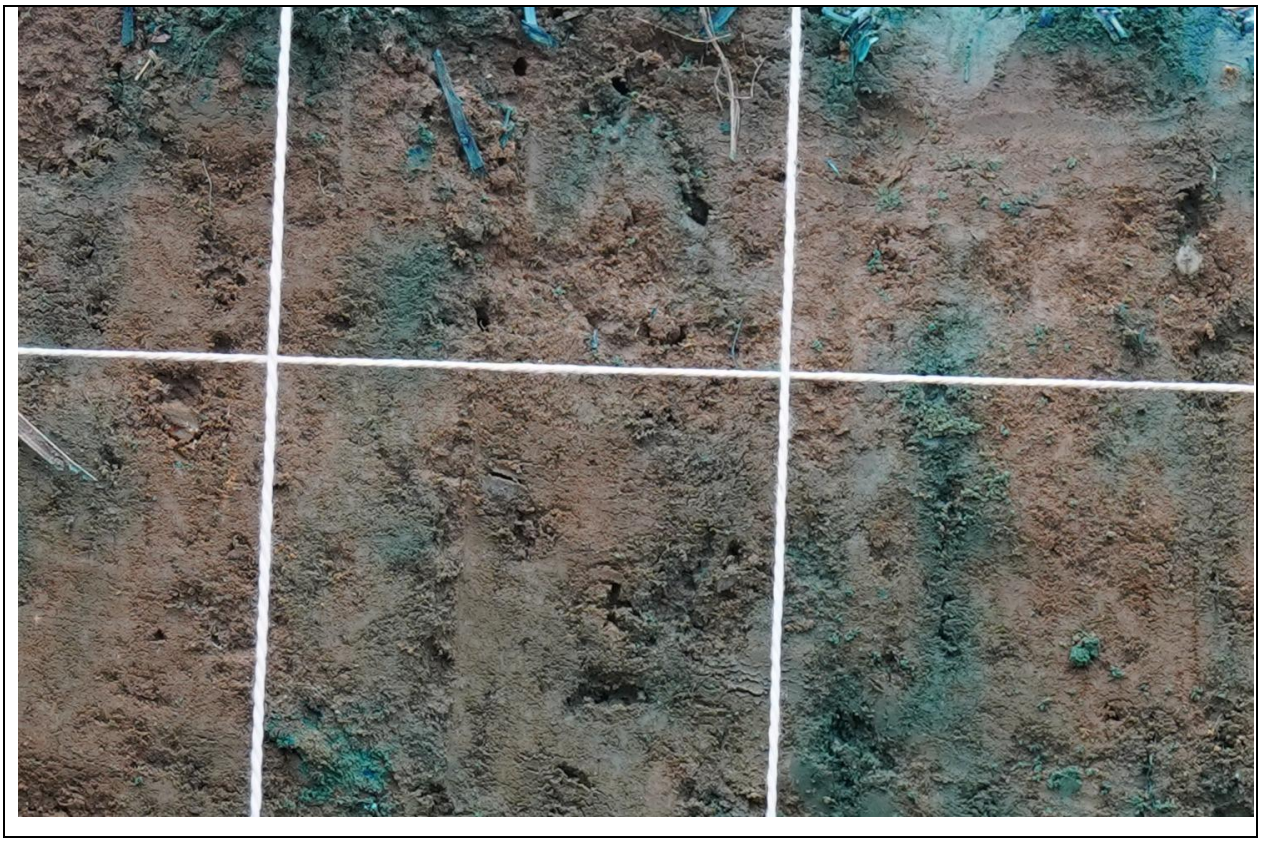

Figure 18. Illustration of earthworm burrows in Field 2, depth 0-20 cm

In summary, the upper soil of field 1 has a relatively high permeability due to plowing, while below 25 cm the permeability decreases significantly. The permeability of the upper soil on field 2 is dominated by earthworm activities, thus leading to increased K_{sat} values.

In field 2, below 25 cm the high permeability is likely due to high earthworm activity, since it is not affected by tillage. This aligns with the findings of Peigné et al. (2009), Crittenden et al. (2014), Chan (2001) and Dekemati et al. (2019), which argue that no-till practice supports earthworm populations in agricultural fields. The low permeability in field 1 at 25 cm can be attributed to the denser plow sole created by ploughing of the upper soil. It is important to note that the abundance of macropore may lead to spatial concentrations of water flow through the soil and therefore will not be described well by a Darcy approach. Furthermore, macropore flow greatly increases the amount of water passing through a porous media and leads to high spatial heterogeneity in the soil (Beven & Germann, 1982). As shown by Alaoui and Helbling (2006), the estimated macropores volume representing only 0.23 to 2% of total soil volume transported approximately 74 to 100% of total water flow.

4. SUMMARY AND CONCLUSIONS

The findings of this study underscore the complex dynamics governing microplastic transport and retention in soil columns under transient flow conditions.

The results related to laboratory soil columns show that sandy loam, with higher water retention and lower hydraulic conductivity, promotes microplastic retention by extending contact time between particles and soil surfaces. In contrast, loamy sand soils with higher saturated hydraulic conductivity and coarser texture facilitate water movement but reduce microplastic retention. Two imbibition and drainage cycles highlighted distinct retention behaviors of microplastics, with breakthrough curves revealing higher release in the first cycle due to initial drier conditions. This effect diminished in the second cycle as soil moisture increased, enhancing electrostatic interactions and, thus, retention. Modelling in Hydrus-1D using a non-equilibrium, depth-dependent approach demonstrated a good fit for breakthrough curves ($R^2 > 0.60$), yet discrepancies in retention profiles at greater depths indicate potential limitations in capturing deeper particle retention dynamics. Parameter variations from inverse modelling further illustrated differences in microplastic attachment rates and dispersivity across treatments. Soil type, rainfall intensity, and microplastic characteristics collectively influenced transport patterns, with LDPE showing the highest mobility under high-intensity rainfall, likely due to its lower bulk density.

These findings highlight the importance of considering soil texture and hydraulic properties in predicting microplastic behavior in soil. The model's overall fit suggests its utility in simulating microplastic transport but also points to the need for tailored parameters to accommodate specific soil-microplastic interactions.

Concerning field experiments during 6- and 13-month periods, significant differences in their temporal and spatial profiles can be noted. LDPE exhibited high stability, with minimal changes in retention profiles and particle size distributions over time, reflecting its resistance to biodegradation and fragmentation. In contrast, PBAT and starch-based microplastics demonstrated more dynamic behavior. PBAT showed moderate degradation and redistribution, while starch-based microplastics underwent significant biodegradation, fragmentation, and vertical transport, resulting in a more even distribution of smaller particles across soil depths.

Although HYDRUS model captured the retention dynamics of all treatments, differences in model parameters, particularly attachment and detachment coefficients, between laboratory and field conditions highlighted the influence of environmental factors. Field-derived parameters demonstrated broader retention profiles and lower attachment rates, emphasizing the importance of long-term ecological exposure, including wet-dry cycles, natural precipitation, groundwater fluctuations, as well as polymer degradation in shaping microplastic behavior.

Integrating laboratory and field approaches is essential to understand microplastic behavior in soils comprehensively. Laboratory experiments provide controlled environments for isolating specific factors,

while field studies capture the complexity of real-world conditions. Together, these approaches enable the development of hybrid models that more accurately predict the fate of microplastics in diverse soil environments, contributing to improved risk assessments and management strategies for microplastic pollution.

The results of the transport of MP in undisturbed soil under natural conditions show that tillage has a significant impact on soil structure and water flow. Infiltrating water is dominated by diffusive flow in field 1 (till), while in field 2 (no-till) a high abundance of preferential flow pathways was observed. The findings suggests that the microplastic penetration depth is increased with the abundance of biopores, highlighting the importance of preferential flow paths for microplastic mobility in the vadose zone. Furthermore, the results indicate that a large percentage of microplastic fails to penetrate the soil after a period of 5.5 months, which is more pronounced in the tillage field, due to compaction of the topsoil. The highest mobility of plastic particles was detected at a depth of 0-15 cm. However, small amounts of plastic were still found at 45 cm depth, demonstrating the capability of plastic to also infiltrate the soil to deeper layers. To accurately quantify microplastic concentration it is advised to decrease the input concentration on the lysimeter surface to prevent methodical errors. As a part of the MINAGRIS project, additional soil moisture and rain data was collected for further modeling purposes with HYDRUS 1D, which will also be conducted in the scope of the MINAGRIS project.

5. LIST OF REFERENCES

Alaoui, A., Caduff, H. H., Gerke, R., Weingartner R., 2011. Preferential Flow Effects on Infiltration and Runoff in Grassland and Forest Soils. *Vadose Zone Journal*, 10(1), pp. 367-377, doi.org/10.2136/vzj2010.0076

Alaoui, A., Helbling, A., 2006. Evaluation of soil compaction using hydrodynamic water content variation: comparison between compacted and non compacted soil. Geoderma 134, 97–108.

Beven, K., Germann, P., 1982. Macropores and Water Flow in Soils. *Water Resources Research*, 18(5), pp. 1311-1325, doi.org/10.1029/WR018i005p01311

Bradford, S. and Toride, N., 2007. A stochastic model for colloid transport and deposition. Journal of environmental quality, 36(5): 1346-1356.

Chan, K. Y., 2001. An overview of some tillage impacts on earthworm population abundance and diversity – implications for functioning in soil. *Soil and Tillage Research*, 57(4), pp. 179-191, doi.org/10.1016/S0167-1987(00)00173-2

Cheng, T. and Saiers, J.E., 2010. Colloid-facilitated transport of cesium in vadose-zone sediments: The importance of flow transients. Environmental Science & Technology, 44(19): 7443-7449.

Chervet, A., Ramseier, L., Sturny, W. G., Zuber, M., Stettler, M., Weisskopf, P., Zihlmann, U. Martinez, I. G., Keller, T., 2016. Erträge und Bodenparameter nach 20 Jahren Direktsaat und Pflug. Agrarforschung Schweiz, 7(5), pp. 216-223, 35696

Clapp, R. B., Hornberger, G. M., 1978. Empirical equations for some soil hydraulic properties. *Water Resources Research*, 14(4), pp. 601 – 604, doi.org/10.1029/WR014i004p00601

Crittenden, S. J., Eswaramurthy, T., de Goede, R. G. M., Brussaard, L., Pulleman, M. M., 2014. Effect of tillage on earthworms over short- and medium-term in conventional and organic farming. *Applied Soil Ecology*, 83, pp. 140-148, doi.org/10.1016/j.apsoil.2014.03.001

Dekemati, I., Simon, B., Vinogradov, S., Birkás, M., 2019. The effects of various tillage treatments on soil physical properties, earthworm abundance and crop yield in Hungary. *Soil and Tillage Research*, 194, 104334, doi.org/10.1016/j.still.2019.104334

Dong, Z., Zhu, L., Zhang, W., Huang, R., Lv, X. W., Jing, X., Yang, Z., Wang, J., Qiu, Y., 2019. Role of surface functionalities of nanoplastics on their transport in seawater-saturated sea sand. *Environmental Pollution*, 255(1), 113177, doi.org/10.1016/j.envpol.2019.113177

Ervin, J.S. et al., 2013. Characterization of fecal concentrations in human and other animal sources by physical, culture-based, and quantitative real-time PCR methods. Water Research, 47(18): 6873-6882.

Foetisch, A., Grunder, A., Kuster, B., Stalder, T., Bigalke, M., 2024. All black: a microplastic extraction combined with colour-based analysis allows identification and characterization of tire wear particles (TWP) in soils. Microplastics and Nanoplastics, 4(25), doi.org/10.1186/s43591-024-00102-9

Hahn, M.W., Abadzic, D. and O'Melia, C.R., 2004. Aquasols: On the role of secondary minima. Environmental science & technology, 38(22): 5915-5924.

Ly, S., 2025. Investigating Microplastic Transport through Preferential Flow Paths by using Field Data from a Lysimeter based Field Experiment. Master thesis, Institute of Geography, Soil Science Unit, University of Bern.

Mitzel, M.R., Sand, S., Whalen, J.K. and Tufenkji, N., 2016. Hydrophobicity of biofilm coatings influences the transport dynamics of polystyrene nanoparticles in biofilm-coated sand. Water research, 92: 113-120.

Peigné, J., Cannavaciuolo, M., Gautronneau, Y., Aveline, A., Giteau, J. L., Cluzeau, D., 2009. Earthworm populations under different tillage systems in organic farming. *Soil and Tillage Research*, 104 (2), pp. 207-2014, doi.org/10.1016/j.still.2009.02.011

Pradel, A. et al., 2020. Deposition of environmentally relevant nanoplastic models in sand during transport experiments. Chemosphere, 255: 126912.

Ren, Z., Gui, Y., Xu, X., Zhao, L., Qiu, H., Cao, X., 2021. Microplastics in the soil-groundwater environment: Aging, migration, and co-transport of contaminants – A critical review. Journal of Hazardous Materials, 419, 126455, doi.org/10.1016/j.jhazmat.2021.126455

Rhodes, M.J., 2008. Introduction to Particle Technology. John Wiley & Sons.

Shang, J., Flury, M. and Deng, Y., 2009. Force measurements between particles and the air-water interface: Implications for particle mobilization in unsaturated porous media. Water Resources Research, 45(6).

Starr, J. L., Paltineanu, I. C., 2002. Methods for measurement of soil water content: Capacitance devices, in Dane, J. H., Topp, G. C. (eds) Methods of Soil Analysis: Part 4 Physical Methods. Madison, Wisconsin: Soil Science Society of America, Inc.

Taučer-Kapteijn, M., Hoogenboezem, W. and Medema, G., 2016. Environmental growth of the faecal indicator Enterococcus moraviensis. Water Science and Technology: Water Supply, 16(4): 971-979.

Taučer-Kapteijn, M., Hoogenboezem, W., Hoogenboezem, R., De Haas, S. and Medema, G., 2017. Source tracking of Enterococcus moraviensis and E. haemoperoxidus. Journal of Water and Health, 15(1): 41-49.

Tehrani, R.S., Yang, X. and van Dam, J., 2025. Rainfall-induced microplastic fate and transport in unsaturated Dutch soils. Journal of Contaminant Hydrology, 268: 104456.

Tiraferri, A., Tosco, T. and Sethi, R., 2011. Transport and retention of microparticles in packed sand columns at low and intermediate ionic strengths: experiments and mathematical modeling. Environmental Earth Sciences, 63: 847-859.

Tufenkji, N. and Elimelech, M., 2004. Correlation equation for predicting single-collector efficiency in physicochemical filtration in saturated porous media. Environmental science & technology, 38(2): 529-536.

Tufenkji, N. and Elimelech, M., 2005. Breakdown of colloid filtration theory: Role of the secondary energy minimum and surface charge heterogeneities. Langmuir, 21(3): 841-852.

Wang, C., Wang, R., Huo, Z., Xie, E. and Dahlke, H.E., 2020. Colloid transport through soil and other porous media under transient flow conditions—A review. Wiley Interdisciplinary Reviews: Water, 7(4): e1439.

Xu, S., Liao, Q. and Saiers, J.E., 2008. Straining of nonspherical colloids in saturated porous media. Environmental science & technology, 42(3): 771-778.

Yan, X. et al., 2020. Downward transport of naturally-aged light microplastics in natural loamy sand and the implication to the dissemination of antibiotic resistance genes. Environmental Pollution, 262: 114270.

Šimůnek, J., Šejna, M., Saito, H., Sakai, M., van Genuchten, M. Th., 2018. The HYDRUS-1D Software Package for Simulating the One-Dimensional Movement of Water, Heat, and Multiple Solutes in Variably-Saturated Media. Version 4.17, Department of Environmental Sciences University of California Riverside, Riverside, California

6. ANNEXE 1

Table 10. Bulk density values for soil texture classes.

Texture Class	**Bulk density (g cm^{-3})**
Sand	1.65
Loamy sand	1.6
Sandy loam	1.55
Loam	1.5
Sandy clay loam	1.5
Silty clay loam	1.5
Silty loam	1.5
Clay loam	1.45
Silty clay	1.45
Sandy clay	1.4
Clay	1.35

Classes after Zeri et al. (2018)